J. Fluid Mech. (2007), *vol.* 582, *pp.* 223–251.
doi:10.1017/S0022112007005824 Printed in the United Kingdom

An analytical solution for two slender bodies of revolution translating in very close proximity

Q. X. WANG

School of Mathematics, The University of Birmingham, Edgbaston, Birmingham B15 2TT, UK

(Received 13 January 2006 and in revised form 19 January 2007)

The irrotational flow past two slender bodies of revolution at angles of yaw, translating in parallel paths in very close proximity, is analysed by extending the classical slender body theory. The flow far away from the two bodies is shown to be a direct problem, which is represented in terms of two line sources along their longitudinal axes, at the strengths of the variation rates of their cross-section areas. The inner flow near the two bodies is reduced to the plane flow problem of the expanding (contracting) and lateral translations of two parallel circular cylinders with different radii, which is then solved analytically using conformal mapping. Consequently, an analytical flow solution has been obtained for two arbitrary slender bodies of revolution at angles of yaw translating in close proximity. The lateral forces and yaw moments acting on the two bodies are obtained in terms of integrals along the body lengths. A comparison is made among the present model for two slender bodies in close proximity, Tuck & Newman's (1974) model for two slender bodies far apart, and VSAERO (AMI)–commercial software based on potential flow theory and the boundary element method (BEM). The attraction force of the present model agrees well with the BEM result, when the clearance, h_0, is within 20 % of the body length, whereas the attraction force of Tuck & Newman is much smaller than the BEM result when h_0 is within 30 % of the body length, but approaches the latter when h_0 is about half the body length. Numerical simulations are performed for the three typical manoeuvres of two bodies: (i) a body passing a stationary body, (ii) two bodies in a meeting manoeuvre (translating in opposite directions), and (iii) two bodies in a passing manoeuvre (translating in the same direction). The analysis reveals the orders of the lateral forces and yaw moments, as well as their variation trends in terms of the manoeuvre type, velocities, sizes, angles of yaw of the two bodies, and their proximity, etc. These irrotational dynamic features are expected to provide a basic understanding of this problem and will be beneficial to further numerical and experimental studies involving additional physical effects.

1. Introduction

The hydrodynamic interaction between two slender bodies poses an interesting theoretical problem, where the fluid domain is complex and varying with time. Its study is of practical importance in the context of interactions of two marine vessels (cf. Tuck & Newman 1974; Yeung & Hwang 1977; Yeung & Tan 1980; Korsmeyer, Lee & Newman 1993), where the attraction between the two vessels may be comparable to the buoyancies acting on them. It also has applications for high-speed trains moving in very close proximity (cf. Kikuchi, Maeda & Yanagizawa 1996; Yang & Luh 1998; Liu 2004). In fact, the attraction between two trains translating at speeds of 360 mph

in very close proximity may be three orders of magnitude larger than the air buoyancies acting on them (cf. Wang 2005). Applications also include understanding dolphin mother–calf interactions, to identify possible reasons for loss of contact between mother and calf during chases (Weihs 2004).

Numerical modelling of two-body interaction has been performed, mainly based on the potential flow theory and boundary element method, by Landweber, Chwang & Guo (1991), Guo & Chwang (1992), Korsmeyer *et al.* (1993), Kikuchi *et al.* (1996), Yang & Luh (1998), and Fang & Chen (2002), among others. The numerical approach has the advantage of handling general geometry, but it is inaccurate or even singular when the two bodies are in very close proximity (Tuck 1980; Guo & Chwang 1992).

This work concerns the theoretical study of the interaction of two slender bodies using slender body theory. A few decades ago, the slender body theory was one of the most popular theorems in aerodynamics as well as marine hydrodynamics (cf. Munk 1924; Van Dyke 1959; Lighthill 1960; Newman & Wu 1975). Although powerful modern computational capabilities allow us to compute the flow around bodies of arbitrary shapes, slender body theory remains very useful to predict and explain the main features of flow around slender bodies. It has been applied in recent years to analyse flows past slender bodies with complex geometries or physical effects (cf. Faltinsen, Newman & Vinje 1995; Sellier 1997; Becker, Koehler & Stone 2003; Fontaine, Faltinsen & Cointe 2000; Chen, Sharma & Stuntz 2003).

A few theoretical studies on the interaction of two moving slender bodies have been performed based on the classical slender body theory. Tuck & Newman (1974), Yeung & Hwang (1977), Yeung & Tan (1980) and Cohen & Beck (1983) analysed a ship moving near another ship or bank, assuming that the clearance between them was comparable with the ship length. The two bodies are therefore in each other's far-field and their interactions can be approximated using the far-field asymptotic approximations of the slender body theory. Miloh & Hauptman (1980) analysed an elongated spheroid moving near a flat wall or a free surface at low Froude numbers using the Havelock method.

Alternatively, Newman (1965) studied a slender body of revolution at zero incidence moving in very close proximity to a flat wall, by representing the flow in terms of a curved line source along the body, together with its image at the wall. Wang (2005) extended Newman's work to a slender body of revolution at angles of attack and yaw moving in very close proximity to curved ground, using the method of matched asymptotic expansions.

As a development of the above theoretical works, this study concerns the strong interaction between two slender bodies at angles of yaw translating in parallel paths in very close proximity. Owing to the difficult mathematical treatment for arbitrary shaped bodies, this paper is focused on two slender bodies of revolution. We assume that the radii and yaw angles of the two bodies and the clearance between them are of the same order and small quantities compared to their lengths. This work is based on the potential flow theory too, since it provides a good approximation for high-Reynolds-number flows.

The remainder of the paper is organized as follows. In § 2, the flow field is divided into an outer region far away from the two bodies and an inner region near the two bodies, and is analysed using the method of matched asymptotic expansions. The outer flow is shown to be a direct problem. The inner flow is reduced to the plane flow problem of the expanding (contracting) and lateral translations of two parallel circular cylinders, which is then solved analytically using conformal mapping. The formulae for the lateral forces and yaw moments acting on the two bodies are derived

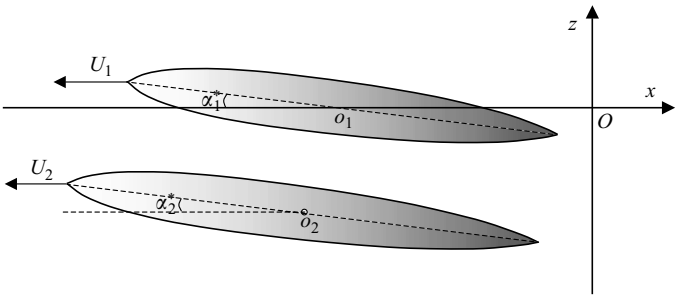

FIGURE 1. The configuration and coordinate system for two slender bodies of revolution at angles of yaw translating on parallel paths in close proximity.

in § 3. In § 4, the analytical results are first compared to those of VSAERO (AMI), a well-validated boundary element modelling, for the case of two equal slender bodies of revolution in symmetrical motion. Numerical analyses are then carried out for the three typical manoeuvres of two bodies: (i) two bodies in a meeting manoeuvre, (ii) two bodies in a passing manoeuvre, and (iii) a body moving near a stationary body. Section 5 contains a summary of this work and conclusions.

2. Analytical flow solution

2.1. *Mathematical modelling*

Consider two slender bodies of revolution at small angles of yaw, translating on parallel paths in very close proximity, as shown in figure 1. The length scale L is chosen as the length of the longer body and the time scale as L/U, where U is the translation speed of the faster body. Normalization is performed for all of the quantities used subsequently. A ground-fixed Cartesian coordinate system O-xyz is defined, with the origin O at the centre of body 1 initially, and the x-axis opposite to the direction of motion of the faster body. Denote the normalized lengths of the two bodies as $2L_1$ and $2L_2$, the angles of yaw as α_1^* and α_2^*, and the normalized translation velocities as $-U_1$ and $-U_2$, respectively.

Let the two bodies start to overlap at $t=0$, when the x-coordinates of their two closer ends are equal. As the x-axis is chosen opposite to the direction of motion of the faster body, the faster body is always behind the slower body initially in the direction of the faster body motion. The passing/meeting period of the two bodies is $2(L_1+L_2)/|U_1-U_2|$. This choice is based on the fact that, to the first-order approximation, two slender bodies interact only when their cross-sections overlap.

Denote x_1 as the x-coordinate relative to the centre $x_{c1}(t)$ of body 1,

$$x_1 = x - x_{c1}(t) = x + U_1 t, \quad x_{c1}(t) = -U_1 t. \tag{1}$$

Denote x_2 as the x-coordinate relative to the centre $x_{c2}(t)$ of body 2. Then, we have

$$x_2 = x - x_{c2}(t), \quad x_{c2}(t) = \begin{cases} L_1 + L_2 - U_2 t & \text{for } |U_1| < |U_2|, \\ -L_1 - L_2 - U_2 t & \text{for } |U_1| \geqslant |U_2|. \end{cases} \tag{2}$$

The initial position of the centre of body 2 is thus $x_{c2}(0) = L_1 + L_2$ when body 2 is the faster body, and is $x_{c2}(0) = -L_1 - L_2$ when body 2 is the slower body.

The surfaces of two bodies, B_1 and B_2, can be expressed as

$$\sqrt{y^2+(x_1\sin\alpha_1^*+z\cos\alpha_1^*)^2}=a_1(x_1\cos\alpha_1^*-z\sin\alpha_1^*) \quad \text{for } |x_1\cos\alpha_1^*-z\sin\alpha_1^*|\leqslant L_1, \tag{3}$$

$$\sqrt{y^2+(x_2\sin\alpha_2^*+z\cos\alpha_1^*+h_0)^2}=a_2(x_2\cos\alpha_2^*-z\sin\alpha_2^*) \quad \text{for } |x_2\cos\alpha_2^*-z\sin\alpha_2^*|\leqslant L_2, \tag{4}$$

where h_0 is the lateral distance between the centres of the two bodies, and $a_1(\xi)$ and $a_2(\xi)$ are the radius distributions of the transverse cross-sections of the two bodies, which are required to be smooth functions and vanished at their noses.

Note that the configuration defined in (1)–(4) is suitable for all three typical manoeuvre cases of two bodies translating on parallel paths: (i) a body moving near a stationary body (where $U_1=0$ or $U_2=0$), (ii) two bodies in a meeting manoeuvre ($U_1U_2<0$), and (iii) two bodies in a passing manoeuvre ($U_1U_2>0$).

This problem can be modelled using slender body theory for two situations. One is when the clearance between the two bodies is comparable with the body lengths, and consequently the two bodies are in each other's far field. Their interactions can be approximated using the far-field asymptotic approximations of the slender body theory. This situation has been studied by Tuck & Newman (1974), Yeung & Hwang (1978), Yeung & Tan (1980) and Cohen & Beck (1983).

The other situation to be studied here is when the two slender bodies are in each other's near field. The minimum longitudinal scale of the problem is the length of the longer body, and the transverse scale B is the lateral distance between their centres plus the sum of the maximum radii. When considering both the bodies in the near field, one must assume that the transverse scale B is much smaller than the horizontal scale L, i.e.

$$\frac{B}{L}=O(\varepsilon),\ \varepsilon\ll 1. \tag{5}$$

This implies that the angles of yaw α_1^*, α_2^* and normalized radii $a_1(x)$, $a_2(x)$ of the two bodies, and the normalized transverse distance h_0 between their geometrical centres are small quantities, which we assume of the same order,

$$a_1(x),\ a_2(x),\ \alpha_1^*,\ \alpha_2^*,\ h_0=O(\varepsilon). \tag{6a}$$

We therefore can express those quantities as

$$(a_1(x),\ a_2(x),\ \alpha_1^*,\ \alpha_2^*,\ h_0)=\varepsilon(A_1(x),\ A_2(x),\ \alpha_1,\ \alpha_2,\ H_0), \tag{6b}$$

where $A_1(x)$, $A_2(x)$, α_1, α_2, $H_0=O(1)$.

The slenderness parameter ε should be chosen as the ratio of B/L, but it varies with the relative positions of the two bodies. With assumption (6a), ε can be chosen as the ratio of the maximum diameter D to the length L of the longer body.

We also introduce the physical assumptions that the fluid is inviscid and incompressible, and the flow is irrotational. A velocity potential $\varphi(x,y,z,t)$ thus exists in the fluid domain bounded by the two bodies, and satisfies the Laplace equation in the fluid domain

$$\frac{\partial^2\varphi}{\partial x^2}+\frac{\partial^2\varphi}{\partial y^2}+\frac{\partial^2\varphi}{\partial z^2}=0, \tag{7a}$$

subject to the following boundary conditions: $\nabla\varphi$ is required to vanish at infinity; the impermeable boundary conditions on the surfaces of the two bodies are

$$y\frac{\partial\varphi}{\partial y}+(x_1\sin\alpha_1^*+z\cos\alpha_1^*)\cos\alpha_1^*\frac{\partial\varphi}{\partial z}$$
$$=a_1a_{1x}\left(U_1+\frac{\partial\varphi}{\partial x}\right)\cos\alpha_1^*-\left(U_1+\frac{\partial\varphi}{\partial x}\right)(x_1\sin\alpha_1^*+z\cos\alpha_1^*)\sin\alpha_1^*\quad\text{on } B_1, \tag{7b}$$

$$y\frac{\partial\varphi}{\partial y}+(x_2\sin\alpha_2^*+z\cos\alpha_2^*+h_0)\cos\alpha_2^*\frac{\partial\varphi}{\partial z}$$
$$=a_2a_{2x}\left(U_2+\frac{\partial\varphi}{\partial x}\right)\cos\alpha_2^*-\left(U_2+\frac{\partial\varphi}{\partial x}\right)(x_2\sin\alpha_2^*+z\cos\alpha_2^*+h_0)\sin\alpha_2^*\quad\text{on } B_2. \tag{7b}$$

The above assumptions appear reasonable for flow problems of large marine vessels and very high-speed trains, which are usually streamlined slender bodies. The Reynolds numbers R_e of these flow problems in terms of body length L are often of $O(10^9)$ or larger, and consequently thin turbulent boundary layers surround the bodies. The thickness of the boundary layer around the forebody of a slender body can be estimated qualitatively as that of a flat plate (cf. Saltzman & Fisher 1970), because the flow is dominant in the longitudinal direction, along which the curvature of the body surface and pressure gradient are small. The maximum thickness δ_m of the boundary layer is thus estimated as $\delta_m=0.37Re^{-0.2}L\leqslant 0.006L$, for $Re\geqslant 10^9$ (cf. Sellier 1997, Ch. 21). The interaction of two slender bodies can be modelled approximately using potential flow theory coupled with boundary layer theory when the minimum clearance C_{min} between the two bodies is larger than δ_m, say four times, i.e. $C_{min}\geqslant 0.024L$. Under this condition, the maximum displacement thickness δ_d of the boundary layer, estimated as $\delta_d=0.036Re^{-0.2}L\leqslant 0.0006L$ for $Re\geqslant 10^9$, is two orders of magnitude smaller than the clearance and the transverse scale of the bodies. The mass flux between the two bodies is not affected significantly by the viscous effects within the boundary layer, and consequently the boundary condition for the irrotational flow can be approximately satisfied on the body surfaces. In addition, the condition on the minimum clearance may be violated locally without destroying the validity of the potential flow solution as a whole (Van Dyke 1975; Wang 2005).

This analysis is based on potential flow theory, because the major forces that affect the motion of a marine vessel near a bank, seabed or another vessel are generated by the irrotational part of the flow (cf. Yeung & Hwang, 1977; Yeung & Tan 1980; Korsmeyer *et al.* 1993). However, a trailing vortex may originate from the sharp edge at the end of the body, which will be associated with the lift force perpendicular to the vortex sheet and can be approximated using lifting surface theory (Newman 1975). An extension of slender body theory to account for the interaction of the afterbody with vortex sheets shed upstream from appendages has been carried out by Newman & Wu (1973). In principle, these works can be applied to the present work for two slender bodies moving in very close proximity. This analysis is invalid when significant boundary layer separation occurs.

2.2. *Inner expansion*

To perform the matched asymptotic expansions, we divide the fluid domain into two regions, the inner region containing the two bodies where x is of $O(1)$, y, z at $O(\varepsilon)$, and the outer region far away from the two bodies where x, y and z are of $O(1)$.

Introduce the inner variables

$$x = x, \quad Y = \frac{y}{\varepsilon}, \quad Z = \frac{z + \alpha_1^* x_1}{\varepsilon}. \tag{8}$$

The boundary value problem (7) can be approximated as follows:

$$\frac{\partial^2 \varphi}{\partial Y^2} + \frac{\partial^2 \varphi}{\partial Z^2} + O\left(\varepsilon^2 \frac{\partial^2 \varphi}{\partial x^2}\right) = 0, \tag{9a}$$

$$\frac{\partial \varphi}{\partial R} = \varepsilon^2 \left(U_1 \frac{\mathrm{d}A_1(x_1)}{\mathrm{d}x_1} - \alpha_1 U_1 \sin\theta\right) + O\left(\varepsilon^4, \varepsilon^2 \frac{\partial \varphi}{\partial x}, \varepsilon^2 \frac{\partial \varphi}{\partial Z}\right)$$
$$\text{on } R = A_1(x_1) + O(\varepsilon^2) \quad \text{for } |x_1 + O(\varepsilon^2)| \leqslant L_1, \tag{9b}$$

$$\frac{\partial \varphi}{\partial R_2} = \varepsilon^2 \left(U_2 \frac{\mathrm{d}A_2(x_2)}{\mathrm{d}x_2} - \alpha_2 U_2 \sin\theta_2\right) + O\left(\varepsilon^4, \varepsilon^2 \frac{\partial \varphi}{\partial x}, \varepsilon^2 \frac{\partial \varphi}{\partial Z}\right)$$
$$\text{on } R_2 = A_2(x_2) + O(\varepsilon^2) \quad \text{for } |x_2 + O(\varepsilon^2)| \leqslant L_2, \tag{9c}$$

where

$$H(x, t) = H_0 - (\alpha_1 x_1 - \alpha_2 x_2), \tag{10a}$$

$$R = \sqrt{Y^2 + Z^2}, \qquad \tan\theta = \frac{Z}{Y}, \tag{10b}$$

$$R_2 = \sqrt{Y^2 + (Z + H)^2}, \qquad \tan\theta_2 = \frac{Z + H}{Y}. \tag{10c}$$

The first-order inner expansion φ^i is

$$\varphi^i = \hat{\mu}(\varepsilon)(\phi(x, Y, Z, t) + S(x, t)) + o(\hat{\mu}). \tag{11}$$

Substituting (11) into (9*a–c*), one obtains that ϕ satisfies

$$\hat{\mu}\left(\frac{\partial^2 \phi}{\partial Y^2} + \frac{\partial^2 \phi}{\partial Z^2}\right) + o(\hat{\mu}) = 0, \tag{12a}$$

$$\hat{\mu} \frac{\partial \phi}{\partial R} = \varepsilon^2 \left(\frac{\mathrm{d}A_1(x_1)}{\mathrm{d}x_1} U_1 - \alpha_1 U_1 \sin\theta\right) + o(\varepsilon^2, \hat{\mu})$$
$$\text{on } R = A_1(x_1) + O(\varepsilon^2) \quad \text{for } |x_1 + O(\varepsilon^2)| \leqslant L_1, \tag{12b}$$

$$\hat{\mu} \frac{\partial \phi}{\partial R_2} = \varepsilon^2 \left(\frac{\mathrm{d}A_2(x_2)}{\mathrm{d}x_1} U_2 - \alpha_2 U_2 \sin\theta_2\right) + o(\varepsilon^2, \hat{\mu})$$
$$\text{on } R_2 = A_2(x_2) + O(\varepsilon^2) \quad \text{for } |x_2 + O(\varepsilon^2)| \leqslant L_2, \tag{12c}$$

Therefore we must choose

$$\hat{\mu} = \varepsilon^2, \tag{13}$$

and the boundary value problem (12) becomes

$$\frac{\partial^2 \phi}{\partial Y^2} + \frac{\partial^2 \phi}{\partial Z^2} = 0, \tag{14a}$$

$$-\frac{\partial \phi}{\partial n} = \frac{\mathrm{d}A_1(x_1)}{\mathrm{d}x_1} U_1 - \alpha_1 U_1 \sin\theta \quad \text{on } C_1 : R = A_1(x_1), \tag{14b}$$

$$-\frac{\partial \phi}{\partial n} = \frac{\mathrm{d}A_2(x_2)}{\mathrm{d}x_2} U_2 - \alpha_2 U_2 \sin\theta_2 \quad \text{on } C_2 : R_2 = A_2(x_2), \tag{14c}$$

where C_1 and C_2 are the peripheries of the cross-sections of the two bodies.

Satisfying the two-dimensional Laplace equation (14*a*), ϕ can be expressed as follows using the Green formula:

$$\phi(x, Y, Z, t) = \oint_{C_1+C_2} \left(G(Y, Z, Y_0, Z_0) \frac{\partial \phi(x, Y_0, Z_0, t)}{\partial n} - \frac{\partial G(Y, Z, Y_0, Z_0)}{\partial n} \phi(x, Y_0, Z_0, t) \right) \mathrm{d}l(Y_0, Z_0), \tag{15}$$

where

$$G(Y, Z, Y_0, Z_0) = \frac{1}{2\pi} \log \sqrt{(Y - Y_0)^2 + (Z - Z_0)^2}. \tag{16}$$

As $R = \sqrt{Y^2 + Z^2} \to \infty$, $G = (1/2\pi) \log R + O(R^{-1})$ and $G_n = O(R^{-1})$ on C_1 and C_2. Equation (15) thus becomes

$$\begin{aligned} \phi(x, Y, Z, t) &= \frac{\log R}{2\pi} \oint_{C_1+C_2} \frac{\partial \phi(x, Y_0, Z_0, t)}{\partial n} \mathrm{d}l(Y_0, Z_0) + O(R^{-1}) \\ &= -\frac{\log R}{2\pi} \left(\int_0^{2\pi} \left(U_1 \frac{\mathrm{d}A_1(x_1)}{\mathrm{d}x_1} - \alpha_1 U_1 \sin\theta \right) A_1(x_1)\, \mathrm{d}\theta \right. \\ &\quad \left. + \int_0^{2\pi} \left(U_2 \frac{\mathrm{d}A_2(x_2)}{\mathrm{d}x_2} - \alpha_2 U_2 \sin\theta_2 \right) A_2(x_2)\, \mathrm{d}\theta_2 \right) + O(R^{-1}) \\ &= -\left(U_1 A_1(x_1) \frac{\mathrm{d}A_1(x_1)}{\mathrm{d}x_1} + U_2 A_2(x_2) \frac{\mathrm{d}A_2(x_2)}{\mathrm{d}x_2} \right) \log R + O(R^{-1}), \end{aligned} \tag{17}$$

where (14*b*, *c*) are used.

To carry out the matching between the inner region and outer region, following Kevorkian & Cole (1985), we introduce the intermediate variable r_σ

$$r_\sigma = \frac{r}{\sigma(\varepsilon)} = \frac{\varepsilon R}{\sigma(\varepsilon)}, \tag{18}$$

with $\varepsilon \ll \sigma \ll 1$. In the intermediate region, $r_\sigma = O(1)$, $R = O(\sigma/\varepsilon)$, and thus

$$\phi(x, Y, Z, t) = -\left(U_1 A_1(x_1) \frac{\mathrm{d}A_1(x_1)}{\mathrm{d}x_1} + U_2 A_2(x_2) \frac{\mathrm{d}A_2(x_2)}{\mathrm{d}x_2} \right) \log \left(\frac{\sigma r_\sigma}{\varepsilon} \right) + O\left(\frac{\varepsilon}{\sigma} \right). \tag{19}$$

Substituting (13), (19) into (11), one obtains the outer limit of the inner expansion

$$(\varphi^i)^o = \varepsilon^2 \left(-\left(U_1 A_1(x_1) \frac{\mathrm{d}A_1(x_1)}{\mathrm{d}x_1} + U_2 A_2(x_2) \frac{\mathrm{d}A_2(x_2)}{\mathrm{d}x_2} \right) \log \left(\frac{\sigma r_\sigma}{\varepsilon} \right) + S(x, t) \right) + O\left(\frac{\varepsilon^3}{\sigma} \right). \tag{20}$$

2.3. *Outer expansion*

The two slender bodies shrink to the line segments, $|x_1| \leqslant L_1$ and $|x_2| \leqslant L_1$, $y = z = 0$, as seen by an outer observer. The outer expansion φ^o can thus be expressed in terms of the line sources along the two segments with unknown strengths $S_1(\xi)$ and $S_2(\xi)$:

$$\varphi^o(x, y, z, t) = \tilde{\mu}(\varepsilon) \int_{-L_1}^{L_1} \frac{S_1(\xi)\, \mathrm{d}\xi}{\sqrt{(x_1 - \xi)^2 + y^2 + z^2}} + \tilde{\mu}(\varepsilon) \int_{-L_2}^{L_2} \frac{S_2(\xi)\, \mathrm{d}\xi}{\sqrt{(x_2 - \xi)^2 + y^2 + z^2}} + o(\tilde{\mu}). \tag{21}$$

The limit form of (21) as $r = \sqrt{y^2 + z^2} \to 0$ is (cf. Kevorkian & Cole 1985, Ch. 4).

$$\varphi^o = \tilde{\mu}(\varepsilon) G(x, t) - 2\tilde{\mu}(\varepsilon)(S_1(x_1) + S_2(x_2)) \log r + o(\tilde{\mu} r^2), \tag{22}$$

where

$$G(x,t) = S_1(-L_1)\log(2L_1+2x_1) + S_1(L_1)\log(2L_1-2x_1) + \int_{-L_1}^{L_1} \frac{\mathrm{d}S_1(\xi)}{\mathrm{d}\xi}\mathrm{sgn}(x_1-\xi)\log|2\xi-2x_1|\,\mathrm{d}\xi + S_2(-L_2)\log(2L_2+2x_2) + S_2(L_2)\log(2L_2-2x_2) + \int_{-L_2}^{L_2} \frac{\mathrm{d}S_2(\xi)}{\mathrm{d}\xi}\mathrm{sgn}(x_2-\xi)\log|2\xi-2x_2|\,\mathrm{d}\xi. \tag{23}$$

In the intermediate region, $r=\sigma(\varepsilon)r_\sigma$, $r_\sigma = O(1)$, the inner limit of the outer expansion then becomes

$$(\varphi^o)^i = \tilde{\mu}(\varepsilon)G(x,t) - 2\tilde{\mu}(\varepsilon)(S_1(x_1)+S_2(x_2))\log(\sigma r_\sigma) + O(\tilde{\mu}\sigma^2). \tag{24}$$

We then use Van Dyke's matching principle (Van Dyke 1975), i.e. equating the inner limit of the outer expansion (20) to the outer limit of the inner expansion (24) in the intermediate region. The matching yields

$$\tilde{\mu}(\varepsilon) = \varepsilon^2, \tag{25a}$$

$$2(S_1(x_1)+S_2(x_2)) = U_1A_1(x_1)\frac{\mathrm{d}A_1(x_1)}{\mathrm{d}x_1} + U_2A_2(x_2)\frac{\mathrm{d}A_2(x_2)}{\mathrm{d}x_2}, \tag{25b}$$

$$S(x,t) = G(x,t) - 2\log\varepsilon(S_1(x_1)+S_2(x_2)). \tag{25c}$$

Using (25*b*) and noticing that $A_1(x_1)$ and $A_2(x_2)$ may be arbitrary, one further obtains

$$S_1(x_1) = \tfrac{1}{2}U_1A_1(x_1)\frac{\mathrm{d}A_1(x_1)}{\mathrm{d}x_1}, \qquad S_2(x_2) = \tfrac{1}{2}U_2A_2(x_2)\frac{\mathrm{d}A_2(x_2)}{\mathrm{d}x_2}. \tag{26a,b}$$

Equation (26) shows that $4\pi S_1(x_1)$ and $4\pi S_2(x_2)$ are the variation rates of the cross-section areas of the two slender bodies, observed in the ground-fixed coordinate system.

On examining (23), we can assume that near $x_i = \pm L_i$ the source strengths $S_i(x_i)$ tend to zero faster than $[\log(L_i+x_i)]^{-1}$ or $[\log(L_i-x_i)]^{-1}$. Therefore, we have the classical restrictions on the nose and tail shapes defined by

$$\lim_{x_i\to -L_i} A_i(x_i)\frac{\mathrm{d}A_i(x_i)}{\mathrm{d}x_i}\log(L_i+x_i) = 0, \tag{27a}$$

$$\lim_{x_i\to L_i} A_i(x_i)\frac{\mathrm{d}A_i(x_i)}{\mathrm{d}x_i}\log(L_i-x_i) = 0. \tag{27b}$$

To summarize, the outer solution is given by (21), (25*a*) and (26). One can see that the disturbance flow far away from the two slender bodies is axisymmetric, and can be obtained by superposing the disturbances of the two bodies. The disturbance of each body can be represented by a line source distribution along its long axis, with the source strength being the variation rate of its cross-sectional area.

The inner expansion takes the form

$$\varphi^i = \varepsilon^2 G(x,t) - 2\varepsilon^2\log\varepsilon(S_1(x_1)+S_2(x_2)) + \varepsilon^2\phi(x,Y,Z,t) + o(\varepsilon^2), \tag{28}$$

where $G(x,t)$ given in (23), $S_1(x_1)$ and $S_2(x_2)$ are given in (26), and ϕ is governed by (14*a–c*). Examining (14), one can draw the following conclusion. The inner flow problem is reduced to the plane flow problems of two circular cylinders with radii $A_1(x_1)$ and $A_2(x_2)$, expanding (contracting) at speeds $A_{1x}U_1$ and $A_{2x}U_2$, and

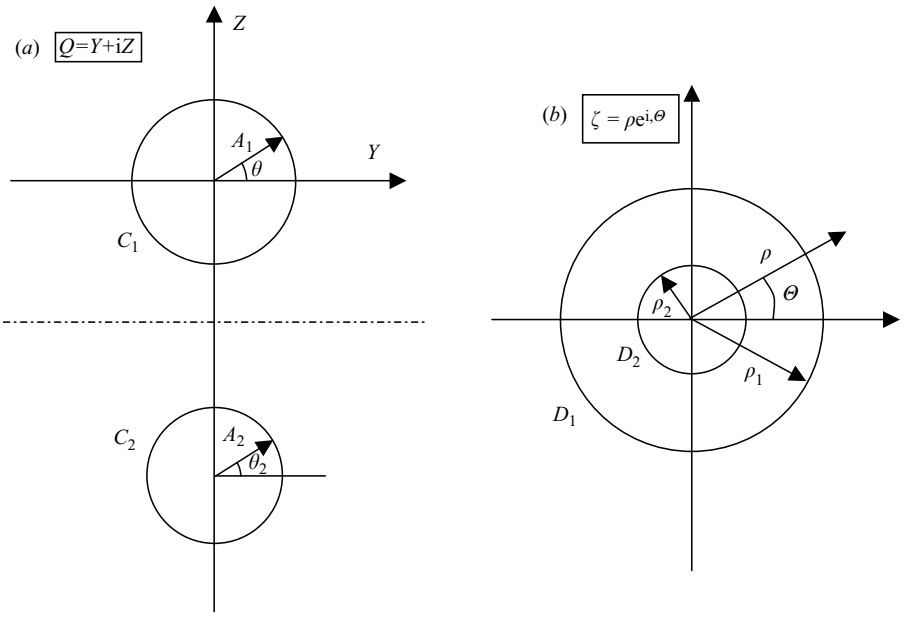

FIGURE 2. The conformal mapping of (a) the domain outside two circles C_1 and C_2 in the $Q = Y + \mathrm{i}Z$ plane to (b) the domain between two concentric circles D_1 and D_2 in the $\varsigma = \rho \mathrm{e}^{\mathrm{i}\Theta}$ plane.

translating laterally at velocities $-\alpha_1 U_1$ and $-\alpha_2 U_2$, respectively. The influence of the deformations, corresponding to the variations of the cross-sectional areas, propagates to the outer region, whereas the influences of angles of yaw are limited to the inner region. The two problems cannot be decoupled like that for a slender body in an unbounded fluid. Wang (2004) obtained the unsteady velocity potential due to two moving circular cylinders in an inviscid fluid. For completeness, the solution of (14) is briefly described in next subsection.

2.4. *Analytical cross-flow solution*

To solve problem (14), a linear fractional conformal mapping is introduced between the cross-flow plane $Q = Y + \mathrm{i}Z$ and the mapped plane $\varsigma = \rho \mathrm{e}^{\mathrm{i}\Theta}$

$$Q = \mathrm{i}C \frac{\varsigma + C}{\varsigma - C} - \mathrm{i}C \coth \beta, \tag{29}$$

where

$$C = \frac{\sqrt{(A_1^2 + A_2^2 - H^2)^2 - 4A_1^2 A_2^2}}{2H}, \quad \beta = \operatorname{arcsinh}(C/A_1). \tag{30a}$$

It maps the domain outside the two circles C_1, $|Q| = A_1$, and C_2, $|Q + H\mathrm{i}| = A_2$, in the cross-flow plane Q, to the domain between the two concentric circles D_1, $|\zeta| = \rho_1$, and D_2, $|\zeta| = \rho_2$, in the mapped plane ς, as sketched in figure 2. Here ρ_1 and ρ_2 are given by

$$\rho_1 = C\mathrm{e}^{\beta}, \quad \rho_2 = C\mathrm{e}^{-\gamma}, \quad \gamma = \operatorname{arcsinh}(C/A_2). \tag{30b}$$

To simplify problem (14), we introduce

$$\phi = 2S_2(x_2) \ln \rho - 2(S_1(x_1) + S_2(x_2)) \log|Q - C| + \Phi. \tag{31}$$

The boundary problem for Φ then becomes

$$\frac{\partial^2 \Phi}{\partial \eta^2} + \frac{\partial^2 \Phi}{\partial \varsigma^2} = 0, \tag{32a}$$

$$\frac{\partial \Phi}{\partial \rho} = 2\frac{S_1 - S_2}{C\mathrm{e}^{\beta}} \frac{1 - \mathrm{e}^{\beta}\cos\Theta}{\mathrm{e}^{2\beta} - 2\mathrm{e}^{\beta}\cos\Theta + 1} + \frac{4\alpha_1 U_1 \mathrm{e}^{\beta}(1 - \cosh\beta\cos\Theta)}{(\mathrm{e}^{2\beta} - 2\mathrm{e}^{\beta}\cos\Theta + 1)^2} \quad \text{on } D_1, \tag{32b}$$

$$\frac{\partial \Phi}{\partial \rho} = 2\frac{S_1 - S_2}{C\mathrm{e}^{-\gamma}} \frac{1 - \mathrm{e}^{\gamma}\cos\Theta}{\mathrm{e}^{2\gamma} - 2\mathrm{e}^{\gamma}\cos\Theta + 1} + \frac{4\alpha_2 U_2 \mathrm{e}^{3\gamma}(1 - \cosh\gamma\ \cos\Theta)}{(\mathrm{e}^{2\gamma} - 2\mathrm{e}^{\gamma}\cos\Theta + 1)^2} \quad \text{on } D_2. \tag{32c}$$

The left-hand sides of (32*b*, *c*) can be further expanded as Fourier series in Θ

$$\frac{\partial \Phi}{\partial \rho} = -2\frac{S_1 - S_2}{C} \sum_{n=1}^{\infty} \frac{\cos(n\Theta)}{\mathrm{e}^{(n+1)\beta}} - \alpha_1 U_1 \sum_{n=1}^{\infty} n \frac{\cos(n\Theta)}{\mathrm{e}^{(n+1)\beta}} \quad \text{on } D_1, \tag{33a}$$

$$\frac{\partial \Phi}{\partial \rho} = -2\frac{S_1 - S_2}{C} \sum_{n=1}^{\infty} \frac{\cos(n\Theta)}{\mathrm{e}^{(n-1)\gamma}} - \alpha_2 U_2 \sum_{n=1}^{\infty} n \frac{\cos(n\Theta)}{\mathrm{e}^{(n-1)\gamma}} \quad \text{on } D_2. \tag{33b}$$

We next assume that the solution of (32) takes the form: $\Phi = \sum_{n=1}^{\infty}(A_n\rho^n + B_n\rho^{-n})\cos(n\Theta)$. Determining its coefficients with (33), and then substituting Φ into (31), we obtain

$$\begin{aligned}\phi = {} & 2S_2 \log\rho - (S_1 + S_2)\log(\rho^2 - 2\rho C\cos\Theta + C^2) \\ & -(S_1 - S_2)\sum_{n=1}^{\infty} \frac{1}{n} \frac{\cos(n\Theta)}{\sinh(n\beta + n\gamma)} \left(\sinh(n\beta)\left(\frac{\rho}{\rho_1}\right)^n - \sinh(n\gamma)\left(\frac{\rho_2}{\rho}\right)^n\right) \\ & -2C\sum_{n=1}^{\infty} \frac{\cos(n\Theta)}{1 - \mathrm{e}^{-2n(\beta+\gamma)}} \left(\mathrm{e}^{-n\beta}(\alpha_1 U_1 - \alpha_2 U_2\,\mathrm{e}^{-2n\gamma})\left(\frac{\rho}{\rho_1}\right)^n \right. \\ & \left. -\mathrm{e}^{-n\gamma}(\alpha_2 U_2 - \alpha_1 U_1\,\mathrm{e}^{-2n\beta})\left(\frac{\rho_2}{\rho}\right)^n\right).\end{aligned} \tag{34}$$

The two series in (34) are absolutely convergent in the whole cross-flow domain, corresponding to $\rho_2 \leqslant \rho \leqslant \rho_1$ and $0 \leqslant \Theta < 2\pi$.

For a transverse plane x, where only one of the two bodies exists, (34) is simplified as follows:

$$\phi = -2\frac{A_1(x_1)S_1(x_1)}{R} - \frac{\alpha_1 U_1 A_1^2(x_1)}{R}\sin\theta \quad (\text{only body 1}), \tag{35a}$$

$$\phi = -2\frac{A_2(x_2)S_2(x_2)}{R_2} - \frac{\alpha_2 U_2 A_2^2(x_2)}{R_2}\sin\theta_2 \quad (\text{only body 2}). \tag{35b}$$

3. Formulae for lateral force and yaw moment

In this section, the formulae for the lateral forces and yaw moments acting on two slender bodies of revolution moving in close proximity are derived. We only consider the force and moment on one of the two bodies, because the force and moment on the other can be simply obtained by rotating the parameters between them.

Having obtained the inner expansion of the potential, the hydrodynamic pressure near the two slender bodies can be obtained using Bernoulli's equation. In the

ground-fixed system $(x, y, z; t)$, the pressure can be expressed as

$$\frac{p}{\rho_f} = -\frac{\partial \varphi^i}{\partial t} - \frac{1}{2}\left(\left(\frac{\partial \varphi^i}{\partial x}\right)^2 + \left(\frac{\partial \varphi^i}{\partial y}\right)^2 + \left(\frac{\partial \varphi^i}{\partial z}\right)^2\right). \tag{36}$$

To calculate the hydrodynamic load, we need to express the pressure in the system $(x_1, Y, Z; t_1)$ fixed to body 1, where x_1 is defined in (1), Y and Z are defined in (8), and $t_1 = t$. Using the relation between the two systems, we have

$$\left.\begin{aligned} &\frac{\partial}{\partial t} = \frac{\partial}{\partial t_1} + U_1\frac{\partial}{\partial x_1} + \alpha_1 U_1 \frac{\partial}{\partial Z}, \\ &\frac{\partial}{\partial x} = \frac{\partial}{\partial x_1} + \alpha_1 \frac{\partial}{\partial Z}, \quad \frac{\partial}{\partial y} = \frac{1}{\varepsilon}\frac{\partial}{\partial Y}, \quad \frac{\partial}{\partial z} = \frac{1}{\varepsilon}\frac{\partial}{\partial Z}. \end{aligned}\right\} \tag{37}$$

Substitution of (37) into (36) yields

$$\begin{aligned} \frac{p}{\rho_f} &= -\frac{\partial \varphi^i}{\partial t_1} - U_1\frac{\partial \varphi^i}{\partial x_1} - \alpha_1 U_1 \frac{\partial \varphi^i}{\partial Z} - \frac{1}{2}\left(\frac{\partial \varphi^i}{\partial x_1} + \alpha_1 \frac{\partial \varphi^i}{\partial Z}\right)^2 - \frac{1}{2\varepsilon^2}\left(\left(\frac{\partial \varphi^i}{\partial Y}\right)^2 + \left(\frac{\partial \varphi^i}{\partial Z}\right)^2\right) \\ &= -\frac{\partial \varphi^i}{\partial t_1} - U_1\frac{\partial \varphi^i}{\partial x_1} - \alpha_1 U_1 \frac{\partial \varphi^i}{\partial Z} - \frac{1}{2\varepsilon^2}\left(\left(\frac{\partial \varphi^i}{\partial Y}\right)^2 + \left(\frac{\partial \varphi^i}{\partial Z}\right)^2\right) + o(\varepsilon^2) \\ &= -\frac{\partial \varphi^i}{\partial t_1} - U_1\frac{\partial \varphi^i}{\partial x_1} - \alpha_1 U_1 \sin\theta \frac{\partial \varphi^i}{\partial R} - \frac{1}{R}\alpha_1 U_1 \cos\theta \frac{\partial \varphi^i}{\partial \theta} \\ &\quad -\frac{1}{2\varepsilon^2}\left(\left(\frac{\partial \varphi^i}{\partial Y}\right)^2 + \left(\frac{\partial \varphi^i}{\partial Z}\right)^2\right) + o(\varepsilon^2). \end{aligned} \tag{38}$$

Substituting the inner expansion (28) into (38), we have

$$\frac{p}{\rho_f} = \varepsilon^2 \log\varepsilon P_0(x_1, t) + \varepsilon^2 P_1(x_1, t) + \varepsilon^2 \quad P(x_1, Y, Z; t) + o(\varepsilon^2), \tag{39a}$$

$$P = -\frac{\partial \phi}{\partial t_1} - U_1\frac{\partial \phi}{\partial x_1} - \alpha_1 U_1 \sin\theta \frac{\partial \phi}{\partial R} - \frac{1}{R}\alpha_1 U_1 \cos\theta \frac{\partial \phi}{\partial \theta} - \frac{1}{2\varepsilon^2}\left(\left(\frac{\partial \phi}{\partial Y}\right)^2 + \left(\frac{\partial \phi}{\partial Z}\right)^2\right). \tag{39b}$$

$P_0(x_1, t)$ and $P_1(x_1, t)$ in (39*a*) depending only on (x_1, t) can be obtained straightforwardly from the terms $G(x, t)$, $S_1(x_1)$ and $S_2(x_2)$ of (28), which have not been given here, since they do not contribute to the lateral force and yaw moment.

The lateral force f_1 on body 1 is given by the integration of $-p\sin\theta$ around the body surface. The yaw moment m_1, to the axis through the body centre and parallel to the y-axis, is given by the integration of $px_1\sin\theta$ around the body surface. Noticing that the terms $P_0(x_1, t)$ and $P_1(x_1, t)$ are cancelled in the integrations, we have

$$\frac{f_1}{\varepsilon^3\rho_f} = -\int_{-L_1}^{L_1} \mathrm{d}x_1 \oint_{C_1} P\sin\theta \mathrm{d}l + o(1), \qquad \frac{m_1}{\varepsilon^3\rho_f} = \int_{-L_1}^{L_1} x_1\,\mathrm{d}x_1 \oint_{C_1} P\sin\theta \mathrm{d}l + o(1). \tag{40a,b}$$

For a transverse plane where only body 1 exists, the inner integral in (40*a*) can be integrated using (35*a*) and (39*b*),

$$-\oint_{C_1} P\sin\theta \mathrm{d}l = \pi A_1 \left(\frac{\partial}{\partial t_1} + U_1\frac{\partial}{\partial x_1}\right)\alpha_1 U_1 A_1 = 2\pi\alpha_1 U_1 S_1(x_1). \tag{41a}$$

For a transverse plane where the two bodies coexist, using (34), we have

$$-\oint_{C_1} P\sin\theta \mathrm{d}l = 2\pi\alpha_1 U_1 S_1 + \oint_{C_1}\left(\frac{\partial}{\partial t_1} + U_1\frac{\partial}{\partial x_1}\right)\phi\sin\theta\,\mathrm{d}l - \frac{\alpha_1 U_1}{A_1}\oint_{C_1}\cos(2\theta)\phi\,\mathrm{d}l + \frac{1}{2}\oint_{C_1}\left(\left(\frac{\partial\phi}{\partial R}\right)^2 + \frac{1}{R^2}\left(\frac{\partial\phi}{\partial\theta}\right)^2\right)\sin\theta\,\mathrm{d}l. \tag{41b}$$

Introduce $J_1(x, t)$, $J_2(x, t)$ and $J_3(x, t)$ as follows:

$$J_1(x,t) = \oint_{C_1}\phi\sin\theta\mathrm{d}l, \tag{42a}$$

$$J_2(x,t) = \oint_{C_1}\phi\cos(2\theta)\,\mathrm{d}l, \tag{42b}$$

$$J_3(x,t) = \frac{1}{2}\oint_{C_1}\left(\left(\frac{\partial\phi}{\partial R}\right)^2 + \frac{1}{R^2}\left(\frac{\partial\phi}{\partial\theta}\right)^2\right)\sin\theta\mathrm{d}l. \tag{42c}$$

Equation (40a) can be expressed as

$$\frac{f_1}{\varepsilon^3\rho_f} = U_1\left(J_1(b,t) - J_1(a,t)\right) + \int_a^b\left(-U_1\frac{J_1}{A_1}\frac{\mathrm{d}A_1}{\mathrm{d}x_1} + \frac{\partial J_1}{\partial t_1} - \frac{\alpha_1 U_1}{A_1}J_2 + J_3\right)\mathrm{d}x_1, \tag{43}$$

where $[a, b]$ is the interval of x_1 in which the cross-sections of both bodies coexist.

The intervals $[a, b]$ are given as follows. For $|U_1| > |U_2|$,

$$a = \begin{cases} -L_1, & \text{for } t \leqslant \dfrac{2L_2}{|U_1 - U_2|}, \\ -L_1 - 2L_2 + (U_1 - U_2)t & \text{for } t > \dfrac{2L_2}{|U_1 - U_2|}, \end{cases} \tag{44a}$$

$$b = \begin{cases} -L_1 + (U_1 - U_2)t & \text{for } t \leqslant \dfrac{2L_1}{|U_1 - U_2|}, \\ L_1 & \text{for } t > \dfrac{2L_1}{|U_1 - U_2|}. \end{cases} \tag{44b}$$

For $|U_1| < |U_2|$,

$$a = \begin{cases} L_1 + (U_1 - U_2)t & \text{for } t \leqslant \dfrac{2L_1}{|U_1 - U_2|}, \\ -L_1 & \text{for } t > \dfrac{2L_1}{|U_1 - U_2|}, \end{cases} \tag{45a}$$

$$b = \begin{cases} L_1, & \text{for } t \leqslant \dfrac{2L_2}{|U_1 - U_2|}, \\ L_1 + 2L_2 + (U_1 - U_2)t & \text{for } t > \dfrac{2L_2}{|U_1 - U_2|}. \end{cases} \tag{45b}$$

Notice that intervals $[a, b]$ given in (44)–(45), where the cross-sections of both bodies coexist, cover all three manoeuvre cases: meeting and passing and a body passing a stationary body.

Similarly to deriving (43), (40*b*) can be expressed as

$$\frac{m_1}{\varepsilon^3\rho_f} = \frac{\alpha_1 U_1 V_1}{2} - U_1(bJ_1(b,t) - aJ_1(a,t)) + \int_a^b \left(-U_1 J_1 - x_1\left(-U_1\frac{J_1}{A_1}\frac{\mathrm{d}A_1}{\mathrm{d}x_1} + \frac{\partial J_1}{\partial t_1} - \frac{\alpha_1 U_1}{A_1}J_2 + J_3\right)\right)\mathrm{d}x_1, \tag{46}$$

where V_1 is the volume of body 1.

$J_1(x,t)$, $J_2(x,t)$ and $J_3(x,t)$ of (42) can be integrated analytically with the following results (see the Appendix for details)

$$J_1(x,t) = 4\pi C\sum_{n=1}^{\infty} a_n \mathrm{e}^{-2n\beta}, \tag{47a}$$

$$J_2(x,t) = 4\pi C\sum_{n=1}^{\infty} (\cosh\beta - n\sinh\beta)a_n \mathrm{e}^{-2n\beta}, \tag{47b}$$

$$J_3(x,t) = \frac{2\pi}{C}\big[-2S_1^2 - 2S_1 b_1 \mathrm{e}^{-\beta}\cosh\beta + 2\sum_{n=1}^{\infty}\big(\cosh\beta \mathrm{e}^{-\beta}(b_n b_{n+1} + a_n a_{n+1}) - \big(b_n^2 + a_n^2\big)\big)\mathrm{e}^{-2n\beta}\big]. \tag{47c}$$

where

$$a_n = S_1 + S_2 - (S_1 - S_2)\frac{1 - 2\mathrm{e}^{-2n\beta} + \mathrm{e}^{-2n(\beta+\gamma)}}{1 - \mathrm{e}^{-2n(\beta+\gamma)}} - Cn\frac{\alpha_1 U_1 - 2\alpha_2 U_2 \mathrm{e}^{-2n\gamma} + \alpha_1 U_1 \mathrm{e}^{-2n(\beta+\gamma)}}{1 - \mathrm{e}^{-2n(\beta+\gamma)}}, \tag{48a}$$

$$b_n = -(2S_1 + Cn\alpha_1 U_1). \tag{48b}$$

$\partial J_1/\partial t_1$ needed in (43) and (46) can be obtained from (47*a*) as follows:

$$\frac{\partial J_1(x,t)}{\partial t_1} = 4\pi\sum_{n=1}^{\infty} n\left(a_n\frac{\partial C}{\partial t_1} + C\frac{\partial a_n}{\partial t_1} - 2nCa_n\frac{\partial \beta}{\partial t_1}\right)\mathrm{e}^{-2n\beta}. \tag{49}$$

$\partial C/\partial t_1$ and $\partial\beta/\partial t_1$ needed in (49) and $\partial\gamma/\partial t_1$ can be obtained from (30):

$$\frac{\partial C}{\partial t_1} = -\frac{C}{H}\frac{\partial H}{\partial t_1} + \frac{\big(A_1^2 + A_2^2 - H^2\big)\left(A_1\alpha_1 U_1 + A_2\alpha_2 U_2 - H\dfrac{\partial H}{\partial t_1}\right) - 2A_1A_2(\alpha_1 U_1 A_2 - \alpha_2 U_2 A_1)}{2H^2 C}, \tag{50a}$$

$$\frac{\partial \beta}{\partial t_1} = \frac{1}{A_1^2\cosh\beta}\left(A_1\frac{\partial C}{\partial t_1} - C\frac{\partial A_1}{\partial t_1}\right), \quad \frac{\partial \gamma}{\partial t_1} = \frac{1}{A_2^2\cosh\gamma}\left(A_2\frac{\partial C}{\partial t_1} - C\frac{\partial A_2}{\partial t_1}\right). \tag{50b,c}$$

$\partial a_n/\partial t_1$ needed in (49) can then be obtained straightforwardly from (48*a*).

The four series in (47) and (49) are absolutely convergent.

4. Numerical analyses

The interaction of two translating slender bodies of revolution modelled in § 3 is calculated using MATLAB. The four series in (47), (49) converge rapidly, since their terms decay exponentially. The four series are summed to a very high accuracy, with the series truncated when the terms are $O(10^{-8})$, since the CPU time needed is minimal. The integrations of the lateral force (43) and pitching moment (46) are performed using recursive adaptive Simpson quadrature. As an illustration, the calculations are performed for the following two slender bodies of revolution:

$$A_1(x_1) = A_1^m \frac{L_1^2 - x_1^2}{L_1^2}, \quad |x_1| \leqslant L_1, \tag{51a}$$

$$A_2(x_2) = A_2^m \frac{L_2^2 - x_2^2}{L_2^2}, \quad |x_2| \leqslant L_2. \tag{51b}$$

The results are given in terms of the dimensionless lateral forces F_1 and F_2, yaw moments M_1 and M_2, and time T:

$$F_i = \frac{f_i}{\rho_f V_{ref}^2 (2L_1)^2 \varepsilon^3}, \quad M_i = \frac{m_i}{\rho_f V_{ref}^2 (2L_1)^3 \varepsilon^3}, \quad i = 1, 2, \tag{52a,b}$$

$$T = \frac{2(L_1 + L_2)t}{|U_1 - U_2|}, \tag{52c}$$

where f_2 and m_2 are the force and moment on body 2. The reference velocity V_{ref} is chosen as U_1 if $U_1 \neq 0$ and as U_2 if $U_1 = 0$. To compare the forces and moments on the two bodies, the same scaling parameters are used for both bodies.

4.1. *Evaluation*

To validate this slender body analysis, its results are compared with those of VSAERO (AMI), well-validated commercial software based on potential flow theory and a three-dimensional boundary element method (BEM) (Maskew 1987; Nathman & Matarrese 2004). The validation is carried out for two equal slender bodies of revolution defined in normalized form as

$$a(x) = 0.05(1 - 4x^2) \quad \text{for} \quad |x| \leqslant 0.5, \tag{53}$$

where the ratio of the maximum diameter to the length of the body is set at 0.1.

VSAERO is only appliable to steady problems. A steady case is thus considered, where the two bodies at the same transverse position move at zero incidence along their long axes at the same velocity U. This problem is equivalent to one of the two bodies moving near a wall at the symmetry plane between the two bodies.

Figure 3(a) shows a comparison between the analytical and numerical results for the normalized lateral force F acting on one of the two bodies versus the lateral distance H_0 between their body centres. Figure 3(b) shows the relative difference between the two results. The forces from the two models agree well for $H_0 \leqslant 0.15$, with the relative difference being less than 5 %, when the maximum transverse dimension across the two bodies B is less than or equal to one quarter of the body length. As H_0 increases, the difference increases rapidly, reaching 20 % for $H_0 = 0.20$, when B is 30 % of the body length. This is as expected. But the difference increases on decreasing H_0 from 0.13 to 0.12. This is possibly because the resolution of the mesh used in the BEM computation is not fine enough for this very close interaction. The

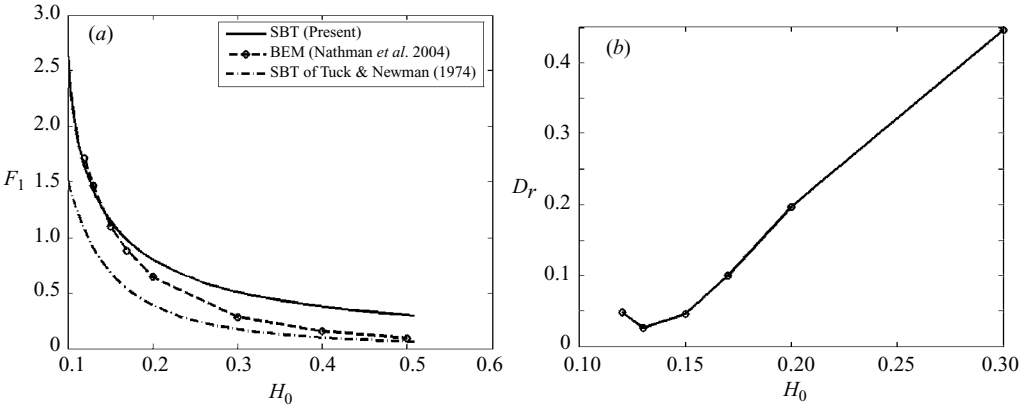

FIGURE 3. (*a*) A comparison of normalized lateral force acting on one of the bodies versus lateral distance among the present slender body theory, the BEM model of VSAERO (AMI) and the slender body theory of Tuck & Newman (1974). (*b*) The relative difference D_r between the results of the present theory and the BEM model.

slender body theory thus provides reasonable results when the minimum clearance between the two bodies is less than $0.1L$.

Figure 3(*a*) also shows the result of Tuck & Newman (1974), which assumes that the two slender bodies are in each other's far field. The attraction found by Tuck & Newman is much smaller than the BEM result when H_0 is within 30 % of the body length, but approaches the latter when H_0 is about half the body length.

4.2. *Meeting manoeuvre*

We now consider the two slender bodies of revolution defined in (51) with the same dimensions in a meeting manoeuvre, where they translate in opposite directions. Figures 4(*a*) and 4(*b*) show the lateral forces F_1 on body 1 and $-F_2$ on body 2 versus time, for lateral distance between their centres $H_0 = 3.0$ and $U_2/U_1 = -1.0$, -1.5 and -2.0. The lateral forces on both bodies have three phases over the meeting period: repulsion, attraction and repulsion. Each phase is about one third of the meeting period under the conditions considered. The peak attraction on each body is significantly larger than the peak repulsion, and the two bodies will tend to be attracted more than repelled, thus giving rise to the danger of a collision. When the speed of body 2 increases, the force on both bodies increases and the force on the slower body increases much faster.

Figures 4(*c*) and 4(*d*) show the yaw moments M_1 on body 1 and M_2 on body 2 versus time for the same case. The moments on both bodies are in four phases: in the bow-out and then bow-in directions during each of the first and second halves of the meeting period. The bow-out and bow-in moments during the first and last phases are consistent with repulsions between the two close ends of the two bodies. In between, the attractions acting on the large middle parts of the two bodies are dominant. The moments are the bow-in (bow-out) direction before (after) the meeting of the centres of the two bodies, when the centre of attraction on each body is at its fore (aft) half. The amplitude of variation of the moment on the slower body is much larger than that on the faster one.

4.3. *Passing manoeuvre*

Secondly, we consider the two slender bodies with the same dimensions in a passing manoeuvre, where they translate in the same direction. Figures 5(*a*) and 5(*b*) show

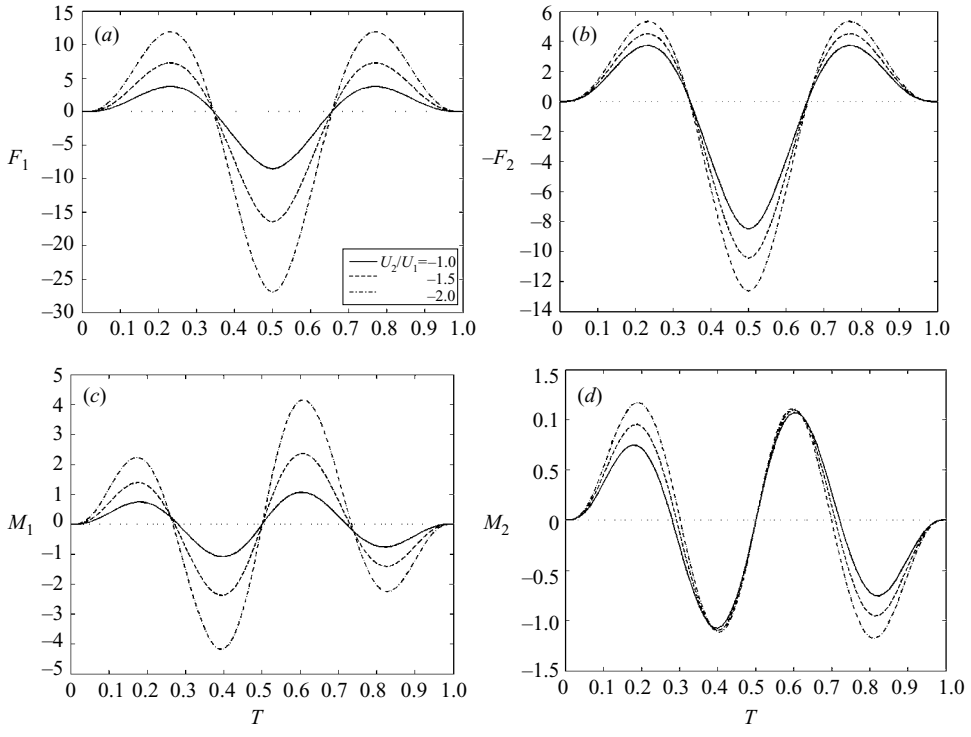

FIGURE 4. (*a*) Lateral force F_1 on body 1 versus time, (*b*) lateral force $-F_2$ on body 2, (*c*) yaw moment M_1 on body 1, (*d*) yaw moment M_2 on body 2, for two slender bodies of revolution in a meeting manoeuvre for $H_0 = 3.0$ and $U_2/U_1 = -1.0$, -1.5 and -2.0.

the lateral forces F_1 and $-F_2$ on the two bodies versus time, for $H_0 = 3.0$ and $U_2/U_1 = 1.001$, 1.5 and 2.0. For $U_2/U_1 = 1.001$, the relative velocity between the two bodies is very small and the unsteady effects are negligible, and hence the results are actually for two bodies in tandem at various relative positions translating at the same speed. As in the meeting manoeuvre (figures 4*a* and 4*b*), the two bodies experience repulsion, attraction and repulsion over the passing period, and the attraction on each body is more dominent than the repulsion. When the speed of body 2 increases, the periods of the three phases for the slower body do not change, whereas the period of attraction for the faster body increases significantly. In fact the faster body experiences attraction for the whole passing period for $U_2/U_1 = 2.0$. Another interesting feature is that the force on the slower body increases with U_2, but the force on the faster body decreases with U_2. As a result, the peak attraction on the slower body is much larger than that on the faster body.

In both meeting and passing manoeuvres, both bodies experience repulsion, attraction and repulsion over the meeting/passing period. This is a well-known feature (cf. Tuck & Newman 1974; Dand 1981; Kikuchi *et al.* 1996; and Vantorre, Laforce & Verzhbitskaya 2001), which is interpreted as follows. When two spheres or two circular cylinders approach (or depart from) each other, they are repelled by the hydrodynamic force (Milne-Thomson 1968; Wang 2004). This is because there is a stagnation point on the axis of symmetry between the two bodies, and a high-pressure zone is generated there. For non-axisymmetric cases, one can expect a lower speed and higher pressure zone between two bodies approaching (or departing from) each

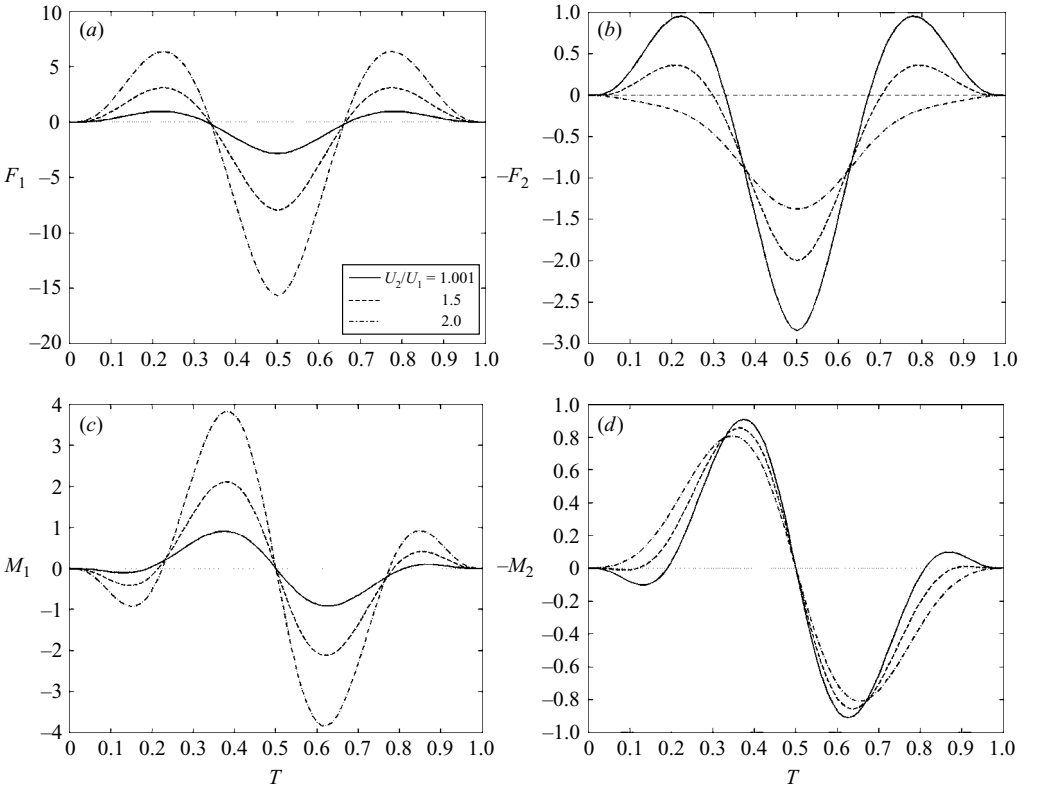

FIGURE 5. (*a*) Lateral force F_1 on body 1 versus time, (*b*) lateral force $-F_2$ on body 2, (*c*) yaw moment M_1 on body 1, (*d*) yaw moment $-M_2$ on body 2, for two slender bodies of revolution in a passing manoeuvre for $H_0 = 3.0$ and $U_2/U_1 = 1.001$, 1.5 and 2.0.

other, and the two bodies experience repulsion forces. In contrast, two bodies passing each other are attracted by the hydrodynamic force, because the flow between them is restricted and moves faster.

Note that figures 4(*a*) and 5(*a*) show that the force, F_1, on the slower body can be substantially larger than that on the faster body. The reason is readily seen when the two-dimensional disturbance velocity field is considered. The more rapidly moving body causes a greater disturbance. As for two slender bodies in a meeting/passing manoeuvre, their two close ends approach (depart from) each other locally during the first (last) part of the passing/meeting period, hence they repel each other. If the two bodies move at different speeds, the stagnation point in the two-dimensional disturbance flow will be closer to the slower one, hence the slower body will experience a higher repelling force. In between the first and last parts of the period, the two bodies pass each other and hence are attracted. The streamlines are diverged more by the faster body and become closer to each other near the slower body. The flow thus moves faster near the slower body and the pressure is lower than near the faster body. Consequently the slower body experiences higher attraction.

Figures 5(*c*) and 5(*d*) show the yaw moments M_1 and $-M_2$ on the two bodies versus time for the same case. An interesting feature is that the moments on both bodies are small during the first and last parts of the passing period, and are thus characterized approximately in only two phases. This feature was observed in the tests

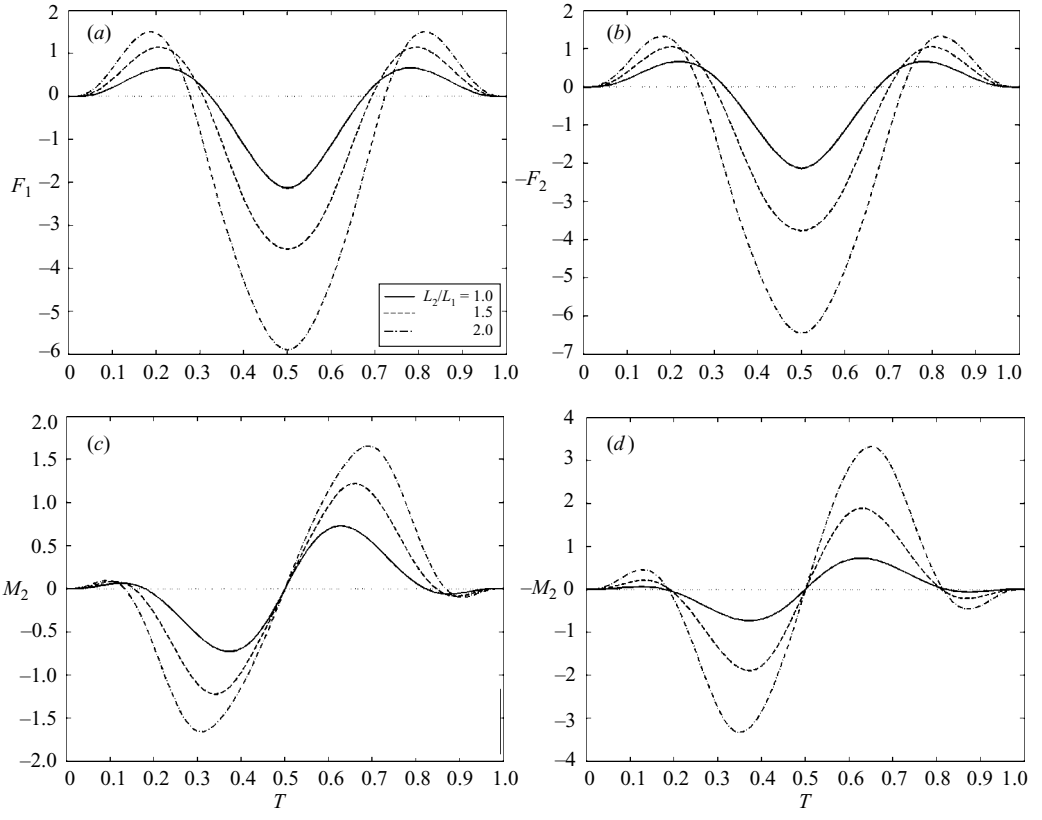

FIGURE 6. (*a*) Lateral force F_1 on body 1 versus time, (*b*) lateral force $-F_2$ on body 2, (*c*) yaw moment M_1 on body 1, (*d*) yaw moment $-M_2$ on body 2, for two slender bodies of revolution in a passing manoeuvre for $U_2 = 0.9U_1$, $H_0 = 3.0$, and $A_2^m/A_1^m = L_2/L_1 =$ 1.0, 1.5 and 2.0.

by Vantorre *et al.* (2001), and is interpreted as follows. The repulsion of on two bodies approaching/departing from each other increases with their relative velocity, whereas the attraction between two bodies passing each other increases with the velocity of the flow between the two bodies. Therefore, the repulsion during the first and last parts of a passing manoeuvre is not as significant as that in a meeting manoeuvre (figures 4*a*, 4*b* and 5*a*, 5*b*), and hence the moments on the two bodies are small at the corresponding times.

The moment on the faster body mainly displays bow-in and bow-out behaviour during the first and second halves of the passing period, and whereas the moment on the slower body displays bow-out and bow-in behaviour during the first and second halves. This 'out-phase' feature is because the passing of the faster body starts from the fore part towards the aft part, and vice versa for the slower body. The peak of the moment on the slower body is much larger than that on the faster one.

Comparing figures 4 and 5, one can see that, at the same speed, the forces on the two bodies in a meeting manoeuvre are much more prominent than those in a passing manoeuvre, whereas the magnitudes of moments are comparable for the two cases.

4.4. *Influence of size, proximity and yaw angle of bodies*

Thirdly, we consider the case where the two bodies are of different sizes. Figures 6(*a*) and 6(*b*) show the lateral forces F_1 and $-F_2$ on the two bodies versus time, when the

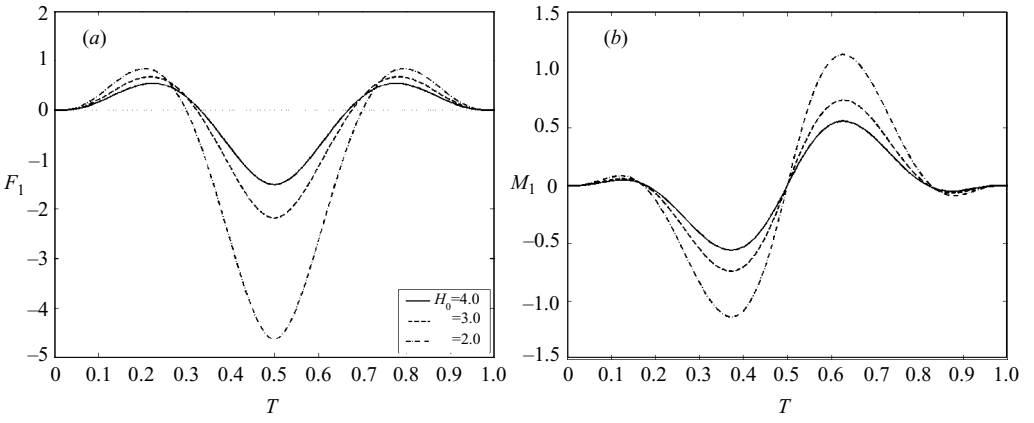

FIGURE 7. (*a*) Lateral force F_1 and (*b*) yaw moment M_1 on body 1 versus time for two slender bodies of revolution in a passing manoeuvre for $U_2 = 0.9U_1$ and various lateral distances $H_0 = 2.0$, 3.0 and 4.0.

two bodies are in a passing manoeuvre for $U_2 = 0.9U_1$, $H_0 = 3.0$, and various values of $A_2^m/A_1^m = L_2/L_1 = 1.0$, 1.5 and 2.0. Both bodies experience repulsion, attraction and repulsion over the passing period. When the size of body 2 increases, the peak attraction on each body increases faster than the peak repulsion, and the period of attraction increases too.

Figures 6(*c*) and 6(*d*) show the yaw moments M_1 and $-M_2$ on the two bodies versus time for this case, which appear mainly in two phases. The faster body experiences the bow-in and bow-out moment during the first and second halves of the passing period, and vice versa for the slower body. As the size of body 2 increases, the amplitude of the moment on the larger body increases faster than that on the smaller body, being about double when $A_2^m/A_1^m = L_2/L_1 = 2.0$.

We now analyse the dynamic effects of the proximity of the two bodies. Figure 7(*a*) shows the lateral force F_1 on body 1 versus time for two bodies with the same dimensions in a passing manoeuvre for $U_2 = 0.9U_1$ and various lateral separation distances $H_0 = 2.0$, 3.0 and 4.0. The bodies experience repulsion, attraction and repulsion over the passing period. The peak attraction increases much faster with the proximity of the two bodies than the peak repulsion. The period of attraction increases with the proximity too. Figure 7(*b*) shows the corresponding moment M_1 on body 1 versus time. The moment appears in a bow-in and bow-out variation during the first and second halves of the passing period, and its amplitude increases rapidly with the proximity.

We next investigate the dynamic effects of the angles of yaw of the two bodies. Figure 8 shows the lateral force F_1 on body 1 versus time for $U_2 = 0.9U_1$, $H_0 = 3.0$, and $\alpha_1 = -1.0$, 0, 1.0 and $\alpha_2 = 0$ (figure 8*a*), and $\alpha_1 = 0$ and $\alpha_2 = -1.0$, 0, 1.0 (figure 8*b*). One can see that the force on one body decreases with its yaw angle and that of the other body for the first half of the passing period, but increases with the two angles for the second half. This is because the clearance between the two bodies increases with the angles of yaw for the first half of the passing period, as shown in figure 9, and vice versa for the second half.

4.5. *One body passing a stationary body*

We further consider a special case where one of the two bodies translates and the other is stationary. Figures 10(*a*) and 10(*b*) show the lateral forces F_1 and

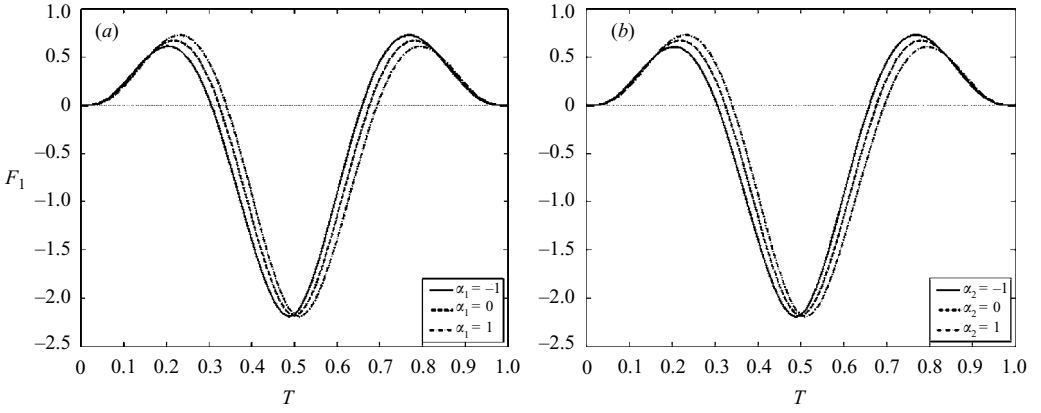

FIGURE 8. Lateral force F_1 on body 1 versus time for the two slender bodies of revolution in a passing manoeuvre for $U_2 = 0.9U_1$, $H_0 = 3.0$, and (*a*) $\alpha_1 = -1.0$, 0, 1.0 and $\alpha_2 = 0$, (*b*) $\alpha_1 = 0$ and $\alpha_2 = -1.0$, 0, 1.0.

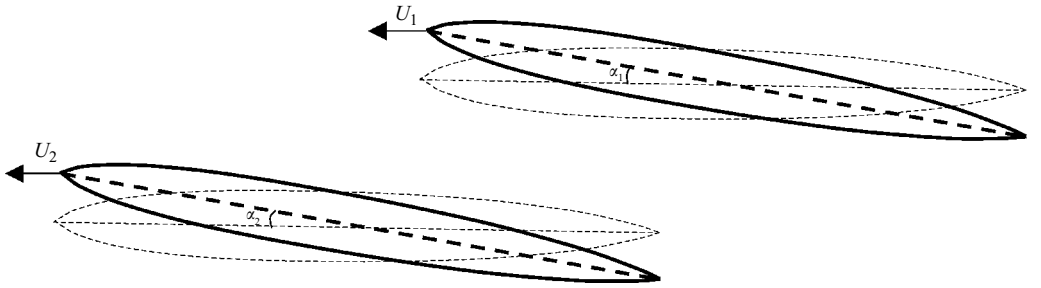

FIGURE 9. The clearance between two slender bodies is shown to increase with the angles of yaw during the first half of the passing period.

$-F_2$ on the two bodies versus time, when body 2 only translates, for $H_0 = 3.0$ and $A_2^m/A_1^m = L_2/L_1 = 0.75$, 1.00 and 1.25. Both bodies experience repulsion, attraction and repulsion over the passing period, as in the passing and meeting manoeuvres (figures 4*a*, 5*a*). The force on the stationary body is significantly larger than that on the moving body. When the two bodies are of the same size, the peak attraction on the stationary body is about 7.2 times that on the moving one. This is important for ships berthed or moored to buoys, since they will experience much greater force than the ship passing them. The moving body experiences a small repulsion at the first and last phases of the passing period (figure 10*b*), because the stagnation point and the resulting high-pressure zone are nearer the stationary body. When the size of body 2 increases, the forces on both bodies increase.

Figures 10(*c*) and 10(*d*) show the yaw moments M_1 and $-M_2$ on the two bodies versus time for the same case. The stationary body 1 experiences the close ends-out yaw moment, in the first and last phases of the passing period (figure 10*c*). In between, it experiences the first meeting ends-in (out) moment at much larger amplitudes before (after) the meeting of the body centres. The moment on the moving body displays the first meeting ends-in and ends-out behaviour in the first and second halves of the passing period (figure 10*d*). These features were noticed in the tests of SSPA (1985) and the calculations of Korsmeyer *et al.* (1993). Comparing the results of figures 10(*c*), 10(*d*), one can see that the amplitude of the moment on the stationary

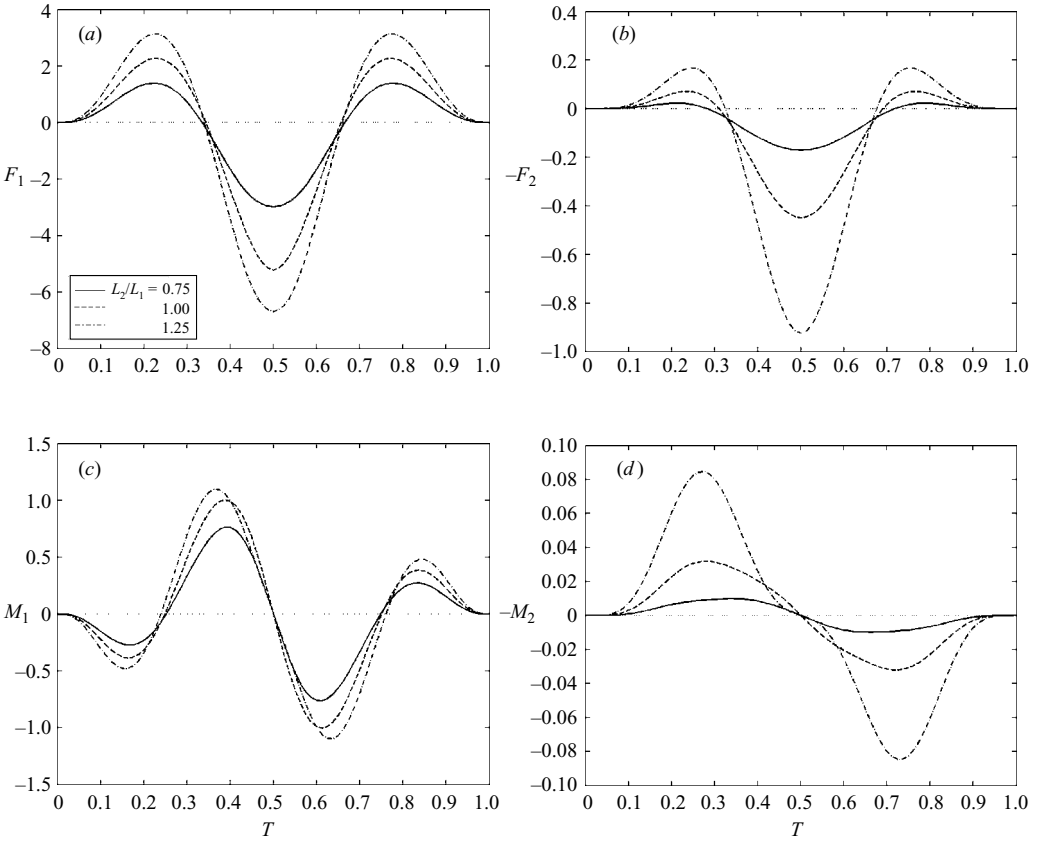

FIGURE 10. (*a*) Lateral force F_1 on body 1 versus time, (*b*) lateral force $-F_2$ on body 2, (*c*) yaw moment M_1 on body 1, (*d*) yaw moment $-M_2$ on body 2, as only body 2 translates and body 1 is stationary for $H_0 = 3.0$ and $A_2^m/A_1^m = L_2/L_1 = 0.75$, 1.00 and 1.25.

body is significantly larger (23 times) than that on the moving body of the same size. When the size of body 2 increases, the amplitudes of the moments on both bodies increase.

4.6. *Maximum magnitudes of forces and moments*

Finally, we analyse the maximum magnitudes of forces and moments acting on the two bodies. Figure 11(*a*) shows the maximum attractions F_{m1} and F_{m2} versus $|U_2/U_1|$, for the two equal slender bodies of revolution moving in close proximity for $H_0 = 3.0$. $|U_2/U_1|$ is chosen in the range of [1, 2], i.e. body 1 being the slower body and body 2 the faster one. As expected $F_{m1} = F_{m2}$ for $|U_2| = |U_1|$. In a meeting manoeuvre ($U_1U_2 < 0$), the maximum attractions on both bodies increase with the ratio $|U_2/U_1|$, the relative velocity between the two bodies, and the maximum attraction on the slower body F_{m1} increases much faster. In a passing manoeuvre ($U_1U_2 > 0$), F_{m1} on the slower body increases rapidly with the relative velocity, whereas F_{m2} on the faster body decreases slowly with the relative velocity. As the result, the maximum attraction on the slower body is much larger than larger that on the faster body in both manoeuvre cases, being 2.1 times for $U_2 = -2U_1$ and 11 times for $U_2 = 2U_1$. It is well known that when two ships are moving in close proximity, the slower ship

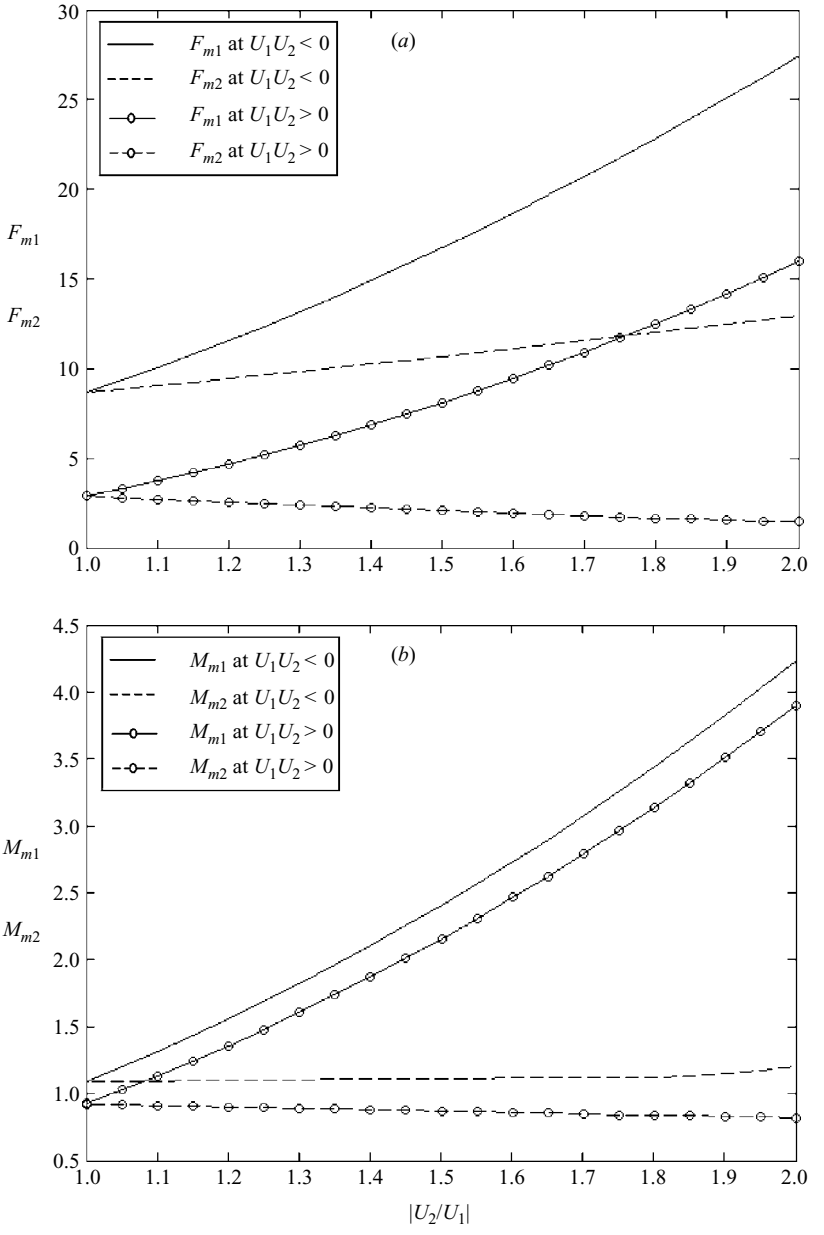

FIGURE 11. (*a*) The maximum magnitudes of the attractions F_{m1} and F_{m2}, and (*b*) the yaw moments M_{m1} and M_{m2}, versus $|U_2/U_1|$, for the two equal slender bodies of revolution moving in close proximity for $H_0 = 3.0$.

experiences a much larger attraction than the faster ship does (see Vantorre *et al.* 2001).

Figure 11(*b*) shows the corresponding maximum magnitudes of the yaw moments M_{m1} and M_{m2} versus $|U_2/U_1|$. In both the meeting manoeuvre and the passing manoeuvre, the moment peak on the slower body M_{m1} increases rapidly with the relative velocity, whereas the moment peak on the faster body M_{m2} varies slightly. Consequently, in both cases, the slower body experiences a much larger moment peak than the faster body, being 3.5 times for $U_2 = -2U_1$ and 4.8 times for $U_2 = 2U_1$.

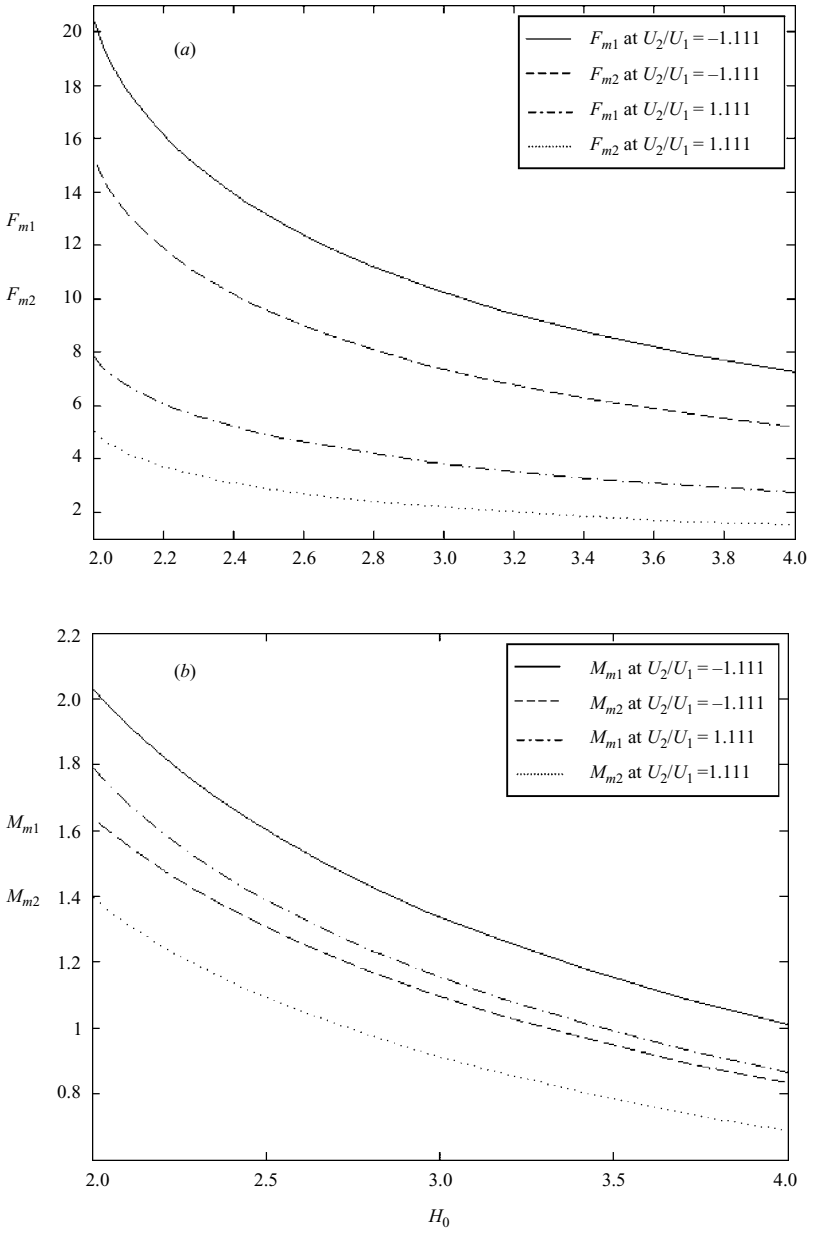

FIGURE 12. (*a*) The maximum magnitudes of the attractions F_{m1} and F_{m2}, (*b*) the yaw moments M_{m1} and M_{m2}, versus H_0, for the two equal slender bodies of revolution moving in close proximity with $|U_2/U_1| = 1.111$.

Figures 11(*a*) and 11(*b*) also compare results of the two types of manoeuvre. One can see that, at the same speeds, the maximum attractions on the two bodies in the meeting manoeuvre are much more prominent than those in the passing manoeuvre, whereas the maximum moments on both bodies in the meeting manoeuvre are only slightly larger than those in the passing manoeuvre.

Figure 12 shows the maximum magnitudes of the attractions F_{m1}, F_{m2} and the yaw moments M_{m1}, M_{m2} versus the lateral distance between the centres of the two bodies

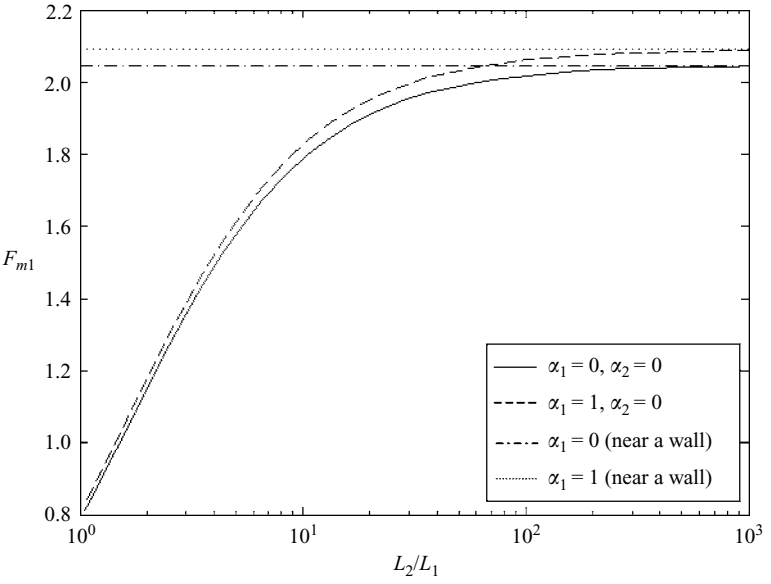

FIGURE 13. The maximum attraction F_{m1} on body 1 versus L_2/L_1 as only body 1 translates and body 2 is stationary, for $H_0 = A_2^m + 2A_1^m$, $A_2^m/A_1^m = L_2/L_1$.

H_0, for the two equal slender bodies of revolution moving in close proximity. The results are shown for the meeting manoeuvre for $U_2/U_1 = -1.111$ and the passing manoeuvre for $U_2/U_1 = 1.111$. In both cases the maximum attractions F_{m1}, F_{m2} and the maximum moments M_{m1}, M_{m2} decrease rapidly with H_0.

Figure 13 shows the maximum attraction F_{m1} on body 1 versus L_2/L_1, when only body 1 translates and body 2 is stationary for $H_0 = A_2^m + 2A_1^m$ and $A_2^m/A_1^m = L_2/L_1$. In this case, body 2 is at zero incidence $\alpha_2 = 0$, while the angle of attack of body 1 is $\alpha_1 = 0$ (solid line) and 1.0 (dashed line). F_{m1} increases with the size of body 2. F_{m1} at $\alpha_1 = 1.0$ is slightly larger than that at $\alpha_1 = 0$. The attractions for a slender body of revolution moving near a wall at the same clearances are also given in the figure. One can see that, when body 2 is significantly larger than body 1, the maximum attraction on body 1 approaches the attraction on the body moving near a wall.

5. Summary and conclusions

An analysis is performed for two slender bodies of revolution in an inviscid fluid translating in very close proximity on parallel paths. We assume that the radii and angles of yaw of the two bodies and the clearance between them are small quantities of the same order, compared to their lengths. Using the method of matched asymptotic expansions, the flow problem is reduced to the plane flow problem of the expanding (contracting) and lateral translations of two parallel circular cylinders, which is then solved using conformal mapping. In addition, the lateral forces and yaw moments acting on the two bodies are obtained in terms of the integrals along the body lengths.

A comparison is performed among the present model, Tuck & Newman's model (1974), and VSAERO (AMI) – commercial software based on potential flow theory and the boundary element method. The present model is for two slender bodies in close proximity, where the clearance between the two bodies is small compared to the body lengths. Tuck & Newman's model is for two slender bodies far apart, where the clearance is comparable to the body lengths, and consequently the two bodies are in each other's far field. Their interactions can be approximated using the far-field asymptotic approximations of the slender body theory.

The test case is for two equal slender bodies with the ratio of diameter to length of 0.1 in symmetrical lateral motion. We compare the attraction between the two bodies versus the lateral distance h_0 between the centres of the two bodies. The attraction of the present model agrees well with that of VSAERO (AMI), when the clearance is small. The relative error is less than 5 % (20 %) when h_0 is within 15 % (20 %) of the body length, whereas the attraction of Tuck & Newman is much smaller than the BEM result when h_0 is within 30 % of the body length, but approaches the latter when h_0 is about a half of the body length.

Numerical analyses are performed for two slender bodies of revolution for the three typical manoeuvres: (i) two bodies in a meeting manoeuvre (translating in opposite directions), (ii) two bodies in a passing manoeuvre (translating in the same direction), and (iii) a body passing a stationary body. The dynamic features found may be summarized as follows, some of which are similar to the known features for two moving slender bodies not in close proximity observed in previous studies.

(1) In all of the three manoeuvres, both bodies experience a sequence of repulsion, attraction and repulsion through the meeting/passing period. The attraction acting on each body is much more prominent than the repulsion, thus giving rise to the danger of a collision of the two bodies.

(2) In a meeting manoeuvre, the yaw moments acting on both bodies are in four phases: in the bow-out and bow-in directions successively during the first and second halves of the meeting period. In a passing manoeuvre, the moments on both bodies have only two phases. The faster body experiences the bow-in and bow-out moment during the first and second halves of the passing period, and vice versa for the slower body.

(3) The forces and moments in a meeting manoeuvre are more prominent than those in a passing manoeuvre. In a meeting manoeuvre, the force and moment on the slower body increase with their relative velocity significantly faster than those on the faster body. In a passing manoeuvre, the force and moment on the slower body increase with the relative velocity, whereas the force and moment on the faster body decreases with the relative velocity. Consequently, the slower body experiences much larger force and moment in both cases. In particular, when one body translates alone and the other is stationary, the force and moment on the stationary body are significantly larger than those on the translating one.

(4) The forces and moments on both bodies increase with their sizes and proximity. The peak attraction on each body increases faster with their sizes and proximity than the peak repulsion does, and the period of attraction increases too. The force on one body decreases with its angle of yaw and that of the other body during the first half of the passing period, but increases with the two angles during the second half.

To obtain the analytical flow solution, the analysis assumes circular cross-sections. However, using the two-dimensional boundary element method the procedure can

be generalized to arbitrary cross-sections. Another possible extension is to include the higher-order approximation following the corresponding works for single slender body (cf. Van Dyke 1959).

This work was partially funded by the Maritime and Port Authority of Singapore. The author would like to express his sincere thanks to Dr J. K. Nathman at Analytical Methods, Inc. (AMI) for his valuable help in providing the simulation results using VSAERO (AMI) used in §4.1. He also wishes to express thanks to Professor D. H. Peregrine for valuable comments.

Appendix. The derivation of (47)

To calculate the three integrals in (42) along the periphery C_1 of the cross-section of body 1 in the cross-flow plane Q, we transform them to those along the corresponding circle D_1 in the mapped plane ζ as follows:

$$J_1 = \oint_{C_1} \phi \sin\theta \mathrm{d}l = \oint_{D_1} \phi \sin\theta J \mathrm{d}l, \tag{A 1}$$

$$J_2 = \oint_{C_1} \phi \cos(2\theta)\, \mathrm{d}l = \oint_{D_1} \phi \cos(2\theta)\, J \mathrm{d}l, \tag{A 2}$$

$$J_2 = \frac{1}{2}\oint_{C_1} \left(\left(\frac{\partial\phi}{\partial R}\right)^2 + \frac{1}{R^2}\left(\frac{\partial\phi}{\partial\theta}\right)^2 \right) \sin\theta \mathrm{d}l$$

$$= \frac{1}{2}\oint_{D_1} \left(\left(\frac{\partial\phi}{\partial\rho}\right)^2 + \frac{1}{\rho^2}\left(\frac{\partial\phi}{\partial\Theta}\right)^2 \right) \sin\theta J^{-1} \mathrm{d}l, \tag{A 3}$$

where $J = |\mathrm{d}Q/\mathrm{d}\zeta|$, $\sin\theta$ and $\cos(2\theta)$ on D_1 can be obtained from the conformal mapping (29)–(30)

$$J|_{D_1} = \frac{2}{\Delta}, \tag{A 4}$$

$$\sin\theta|_{D_1} = -\frac{2\mathrm{e}^{\beta} - (\mathrm{e}^{2\beta}+1)\cos\Theta}{\Delta}, \tag{A 5}$$

$$\cos(2\theta)|_{D_1} = \frac{-\mathrm{e}^{-2\beta}}{2}\left((\mathrm{e}^{4\beta}+1) - 2\frac{(\mathrm{e}^{2\beta}+1)(\mathrm{e}^{2\beta}-1)^2}{\Delta} + \frac{(\mathrm{e}^{2\beta}-1)^4}{\Delta^2} \right), \tag{A 6}$$

where $\Delta = \mathrm{e}^{2\beta} - 2\mathrm{e}^{\beta}\cos\Theta + 1$.

To calculate the integrals in (A 1)–(A 3), we expand φ, φ_Θ and φ_ρ on D_1 in terms of Fourier series in Θ using (34)

$$\phi|_{D_1} = -2S_1 \log\rho_1 + 2\sum_{n=1}^{\infty} a_n \cos(n\Theta)\mathrm{e}^{-n\beta}, \tag{A 7a}$$

$$\phi_\Theta|_{D_1} = -2\sum_{n=1}^{\infty} n a_n \sin(n\Theta)\mathrm{e}^{-n\beta}, \tag{A 7b}$$

$$\rho\phi_\rho|_{D_1} = b_0 + 2\sum_{n=1}^{\infty} b_n \cos(n\Theta)\mathrm{e}^{-n\beta}, \tag{A 7c}$$

where a_n and b_n are given in (48).

To calculate J_1, we express $J\sin\theta$ on D_1 as follows, using (A 4), (A 5):

$$(J\sin\theta)|_{D_1} = -\frac{2\mathrm{e}^{\beta} - (\mathrm{e}^{2\beta}+1)\cos\Theta}{\Delta^2} = \mathrm{e}^{-\beta}\sum_{n=1}^{\infty} n\mathrm{e}^{-n\beta}\cos(n\Theta). \tag{A 8}$$

Substituting (A 7*a*), (A 8) into (A 1) yields

$$\begin{aligned} J_1 &= 2C\int_0^{2\pi}\left(\sum_{n=1}^{\infty} n\mathrm{e}^{-n\beta}\cos(n\Theta)\right)\left(-2S_1\log\rho_1 + 2\sum_{n=1}^{\infty} a_n\mathrm{e}^{-n\beta}\cos(n\Theta)\right)\mathrm{d}\Theta \\ &= 4C\left\{-S_1\log\rho_1\sum_{n=1}^{\infty}\left(n\mathrm{e}^{-n\beta}\int_0^{2\pi}\cos(n\Theta)\,\mathrm{d}\Theta\right)\right. \\ &\quad \left. + \sum_{n,m=1}^{\infty}\left(na_m\mathrm{e}^{-(n+m)\beta}\int_0^{2\pi}\cos(n\Theta)\cos(m\Theta)\,\mathrm{d}\Theta\right)\right\} = 4\pi C\sum_{n=1}^{\infty} na_n\mathrm{e}^{-2n\beta}. \end{aligned} \tag{A 9}$$

In (A 9), we have used the following integral formula:

$$\int_0^{2\pi}\cos(n\Theta)\cos(m\Theta)\,\mathrm{d}\Theta = \pi\delta_{nm} \quad \text{for } n, m \geqslant 1, \tag{A 10}$$

where δ_{nm} is the Kronecker delta, i.e. $\delta_{nm}=0$ for $n\neq m$, and $\delta_{nm}=1$ for $n=m$.

To calculate J_2, we express $J\cos(2\theta)$ on D_1 as follows, using (A 4), (A 6):

$$J\cos(2\theta) = 2\sum_{n=1}^{\infty} f_n\cos(n\Theta)\mathrm{e}^{-n\beta}, \tag{A 11}$$

where

$$f_n = \frac{n}{\mathrm{e}^{\beta}}(\cosh\beta - n\sinh\beta). \tag{A 12}$$

Substituting (A 7*a*), (A 11) into (A 2) yields

$$\begin{aligned} J_2 &= \rho_1\int_0^{2\pi}\left(2\sum_{n=1}^{\infty} f_n\mathrm{e}^{-n\beta}\cos(n\Theta)\right)\left(-2S_1\log\rho_1 + 2\sum_{n=1}^{\infty} a_n\mathrm{e}^{-n\beta}\cos(n\Theta)\right)\mathrm{d}\Theta \\ &= 4\pi\rho_1\sum_{n=1}^{\infty} f_n a_n\mathrm{e}^{-2n\beta} = 4\pi C\sum_{n=1}^{\infty}(\cosh\beta - n\sinh\beta)\,a_n\mathrm{e}^{-2n\beta}. \end{aligned} \tag{A 13}$$

To calculate J_3, we need to calculate the integrant. Using (A 4), (A 5), we have

$$(J^{-1}\sin\theta)|_{D_1} = -\mathrm{e}^{\beta}(1-\cosh\beta\cos\Theta). \tag{A 14}$$

Using (A 7*b*), (A 7*c*), we have

$$\begin{aligned} &\left(\rho^2\left(\frac{\partial\varphi}{\partial\rho}\right)^2 + \left(\frac{\partial\varphi}{\partial\Theta}\right)^2\right)\Bigg|_{D_1} = 4\left\{\sum_{n=1}^{\infty} na_n\sin(n\Theta)\mathrm{e}^{-n\beta}\right\}^2 + \left\{b_0 + 2\sum_{n=1}^{\infty} b_n\cos(n\Theta)\mathrm{e}^{-n\beta}\right\}^2 \\ &= b_0^2 + 4b_0b_1\mathrm{e}^{-\beta}\cos\Theta + 2\sum_{n=1}^{\infty}\sum_{m=1}^{\infty}\mathrm{e}^{-(n+m)\beta}\left\{b_nb_m\left[\cos((n+m)\Theta) + \cos((n-m)\Theta)\right]\right. \\ &\quad \left. + (nma_na_m)\left[\cos((n-m)\Theta) - \cos((n+m)\Theta)\right]\right\}. \end{aligned} \tag{A 15}$$

Substituting (A 14), (A 15) into (A 3) yields

$$
\begin{aligned}
J_3 &= \frac{1}{2\rho_1}\int_0^{2\pi}\left(\rho^2\left(\frac{\partial\varphi}{\partial\rho}\right)^2+\left(\frac{\partial\varphi}{\partial\Theta}\right)^2\right)\Bigg|_{D_1}\sin\theta J^{-1}\,\mathrm{d}\Theta \\
&= \frac{1}{2\rho_1}\int_0^{2\pi}\mathrm{e}^{\beta}(-1+\cosh\beta\cos\Theta)\Bigg(b_0^2+4b_0b_1\mathrm{e}^{-\beta}\cos\Theta \\
&\quad +2\sum_{n=1}^{\infty}\sum_{m=1}^{\infty}(nma_na_m+b_nb_m)\mathrm{e}^{-(m+n)\beta}\cos((n-m)\Theta) \\
&\quad +2\sum_{n=1}^{\infty}\sum_{m=1}^{\infty}(-nma_na_m+b_nb_m)\mathrm{e}^{-(m+n)\beta}\cos((n+m)\Theta)\Bigg)\mathrm{d}\Theta \\
&= \frac{2\pi}{C}\big[-2S_1^2-2S_1b_1\mathrm{e}^{-\beta}\cosh\beta+2\sum_{n=1}^{\infty}\big[\cosh\beta\mathrm{e}^{-\beta}(b_nb_{n+1}+n(n+1)a_na_{n+1}) \\
&\quad -n(n+1)\big(b_n^2+a_n^2\big)\big]\mathrm{e}^{-2n\beta}\big]. \qquad \text{(A 16)}
\end{aligned}
$$

The following integral formulae have been used in the above equations:

$$\int_0^{2\pi}\cos\Theta\cos((n+m)\Theta)\,\mathrm{d}\Theta=0, \qquad \text{(A 17}a\text{)}$$

$$\int_0^{2\pi}\cos\Theta\cos((n-m)\Theta)\,\mathrm{d}\Theta=\begin{cases}0 & \text{for } |n-m|\neq 1,\\ \pi & \text{for } n=m\pm 1,\end{cases} \qquad \text{(A 17}b\text{)}$$

for $n, m \geqslant 1$.

REFERENCES

Becker, L. E., Koehler, S. A. & Stone, H. A. 2003 On self-propulsion of micro-machines at low Reynolds number: Purcell's three-link swimmer. *J. Fluid Mech.* **490**, 15–35.

Chen, X. N., Sharma, S. D. & Stuntz, N. 2003 Zero wave resistance for ships moving in shallow channels at supercritical speeds. Part 2. Improved theory and model experiment. *J. Fluid Mech.* **478**, 111–124.

Cohen, S. B. & Beck, R. F. 1983 Experimental and theoretical hydrodynamic forces on a mathematical model in confined water. *J. Ship Res.* **27**, 75–89.

Dand, I. W. 1981 Some measurements of interaction between ship models passing on parallel courses. *National Maritime Institute, Rep. R*108.

Faltinsen, O. M., Newman, J. N. & Vinje, T. 1995 Nonlinear-wave loads on a slender vertical cylinder. *J. Fluid Mech.* **289**, 179–198.

Fang, M. C. & Chen, G. R. 2002 On three-dimensional solutions of drift forces and moments between two ships in waves. *J. Ship Res.* **46** (4), 280–288.

Fontaine, E., Faltinsen, O. M. & Cointe, R. 2000 New insight into the generation of ship bow waves. *J. Fluid Mech.* **421**, 15–38.

Guo, Z. & Chwang, A. T. 1992 On the planar translation of two bodies in a uniform flow. *J. Ship Res.* **36** (1), 38–54.

Kevorkian, J. & Cole, J. D. 1985 *Perturbation Methods in Applied Mechanics*. Springer.

Kikuchi, K., Maeda & Yanagizawa, T. M. 1996 Numerical simulation of the phenomena due to the passing-by of two bodies using the unsteady boundary element method. *Intl J. Numer. Meth. Fluids* **23** (5), 445–454.

Korsmeyer, F. T., Lee, C. H. & Newman, J. N. 1993 Computation of ship interaction in restricted waters. *J. Ship Res.* **37** (4), 298–306.

Landweber, L., Chwang, A. T. & Guo, Z. 1991 Interaction between two bodies translating in an inviscid fluid. *J. Ship Res.* **35** (1), 1–8.

LIGHTHILL, M. J. 1960 Note on the swimming of slender fish. *J. Fluid Mech.* **9**, 305.

LIU, J. L. 2004 Computations of two passing-by high-speed trains by a relaxation overset-grid algorithm. *Intl J. Numer. Meth. Fluids* **44** (12), 1299–1315.

MASKEW, B. 1987 Program VSAERO theory document. *NASA CR*-4023.

MILNE-THOMSON, L. M. 1968 *Theoretical Hydrodynamics*. MacMillan, London.

MILOH, T. & HAUPTMAN, A. 1980 Large-amplitude motion of an elongated body in shallow-water. *J. Ship. Res.* **24** (4), 256–270.

MUNK, M. M. 1924 The aerodynamic forces on airship hulls. *NACA Rep.* 184.

NATHMAN, J. K. & MATARRESE, M. 2004 Hybrid grid (structured and unstructured) calculations with a potential-based panel method. *AIAA Paper* 2004-4836.

NEWMAN, J. N. 1965 The force and moment on a slender body of revolution moving near a wall. *Naval Ship R. & D. Centre Rep.* 2127.

NEWMAN, J. N. & WU, T. Y. 1973 A generalized slender-body theory for fish-like form. *J. Fluid Mech.* **57**, 673–697.

SALTZMAN, E. J. & FISHER, D. F. 1970 Some turbulent boundary-layer measurements obtained from the forebody of an airplane at Mach numbers up to 1.72. *NASA TN* D-5838.

SCHLICHTING, H. 1979 *Boundary-Layer Theory*. McGraw-Hill.

SELLIER, A. 1997 A general and formal slender-body theory in the non-lifting case. *Proc. R. Soc. Lond.* A **453**, 1733–1751.

SSPA 1985 Model tests performed for CAOF PANAMA Canal Project. *SSPA Rep.* 3062. Swedish State Maritime Centre, Goteborg.

TUCK, E. O. 1978 Hydrodynamic problems of ships in restricted water. *Annu. Rev. Fluid Mech.* **10**, 33–44.

TUCK, E. O. 1980 A Nonlinear Unsteady one-dimensional theory for wings in extreme ground effect. *J. Fluid Mech.* **98**, 33–47.

TUCK, E. O. & NEWMAN, J. N. 1974 Hydrodynamic interactions between ships. *Proc. 10th Symp. Naval Hydr.*, pp. 35–70. Cambridge, Mass. Proceedings, Office of Naval Research, Washington, D.C.

VAN DYKE, M. D. 1959 Second-order theory-axisymmetric flow. *Tech. Rep. NASA* R-47.

VAN DYKE, M. D. 1975 *Perturbation Methods in Fluid Mechanics*. 2nd Edn. The Parabolic Press, Stanford, California.

VANTORRE, M., LAFORCE, E. & VERZHBITSKAYA, E. 2001 Model test based formulations of ship-ship interaction force for simulation purpose. *Proc. 28th Annual General Meeting of Intl Maritime Simulation Forum (IMSF) (Genova, Italy)*.

WANG, Q. X. 2004 Interaction of two circular cylinders in inviscid fluid. *Phys. Fluids* **16** (12), 4412–4425.

WANG, Q. X. 2005 Analyses of a slender body moving near a curved-ground. *Phys. Fluids* **17** (9), 097102.

WEIHS, D. 2004 The hydrodynamics of dolphin drafting. *J. Biol.* **3** (2), 1–5.

YANG, S. A. & LUH, P. A. 1998 A numerical simulation of hydrodynamic forces of ground-effect problem using Lagrange's equation of motion. *Intl J. Numer. Meth. Fluids* **26** (6), 725–747.

YEUNG, R. W. & HWANG, W. Y. 1977 Nearfield hydrodynamics and interactions of ships in shallow water. *J. Hydronautics* **11** (4), 128–135.

YEUNG, R. W. & TAN, W. T. 1980 Hydrodynamic interactions of ships with fixed obstacles. *J. Ship Res.* **24** (1), 50–59.